Quaternary Science Reviews 114 (2015) 203–227

Contents lists available at ScienceDirect

Quaternary Science Reviews

journal homepage: www.elsevier.com/locate/quascirev

Cova del Rinoceront (Castelldefels, Barcelona): a terrestrial record for the Last Interglacial period (MIS 5) in the Mediterranean coast of the Iberian Peninsula

J. Daura [a, b, *], M. Sanz [a, b], R. Julià [c], D. García-Fernández [a], J.J. Fornós [d], M. Vaquero [e, f], E. Allué [e, f], J.M. López-García [g], H.A. Blain [e, f], J.E. Ortiz [h], T. Torres [h], R.M. Albert [i, j], À. Rodríguez-Cintas [i], A. Sánchez-Marco [k], E. Cerdeño [l], A.R. Skinner [m], Y. Asmeron [n], V.J. Polyak [n], M. Garcés [o], L.J. Arnold [p], M. Demuro [q], A.W.G. Pike [r], I. Euba [s], R.F. Rodríguez [a], A.S. Yagüe [a], L. Villaescusa [a], S. Gómez [a], A. Rubio [a, t], M. Pedro [a], J.M. Fullola [b], J. Zilhão [b, j]

[a] GRQ, Grup de Recerca del Quaternari, SERP, Dept. Prehistòria, H. Antiga i Arqueologia, Facultat de Geografia i Història, Universitat de Barcelona, C/Montalegre, 6, 08001 Barcelona, Spain
[b] SERP, Dept. Prehistòria, H. Antiga i Arqueologia, Facultat de Geografia i Història, Universitat de Barcelona, C/Montalegre, 6, 08001 Barcelona, Spain
[c] Institut Ciències de la Terra "Jaume Almera", CSIC, C/Lluís Solé Sabarís s/n, Barcelona 08028, Spain
[d] Departament de Ciències de la Terra, Universitat de les Illes Balears, Ctra. Valldemossa km 7, 5, 07122 Illes Balears, Spain
[e] IPHES, Institut Català de Paleoecologia Humana i Evolució Social, C/Escorxador s/n, 43003 Tarragona, Spain
[f] Àrea de Prehistòria, Universitat Rovira i Virgili (URV), Avinguda de Catalunya 35, 43002 Tarragona, Spain
[g] Sezione di Scienze Preistoriche e Antropologiche, Dipartamento di Studi Umanistici, Università degli Studi di Ferrara, C.so Ercole 1 d'Este 32, 44121 Ferrara, Italy
[h] Laboratorio de Estratigrafía Biomolecular, Departamento de Ingeniería Geológica, Escuela Técnica Superior de Ingenieros de Minas, Universidad Politécnica de Madrid C/Rios Rosas 21, 28003 Madrid, Spain
[i] ERAAUB, Equip de Recerca Arqueològica i Arqueomètrica de la Universitat de Barcelona, Departament de Prehistòria, Història Antiga i Arqueologia, Universitat de Barcelona, Carrer Montealegre, 6, 08001 Barcelona, Spain
[j] ICREA, Catalan Institution for Research and Advanced Studies, Spain
[k] ICP, Institut Català de Paleontologia Miquel Crusafont, Campus de la UAB, 08193 Bellaterra, Spain
[l] Paleontología, IANIGLA, CCT-CONICET-Mendoza, Avenida Ruiz Leal s/n, 5500 Mendoza, Argentina
[m] Chemistry Department, Williams College, 47 Lab Campus Drive, 01267 Williamstown, MA, USA
[n] Department of Earth & Planetary Sciences, University of New Mexico, Albuquerque, 87131 New Mexico, USA
[o] Grup de Geodinamica i Analisis de Conques (GGAC), Universitat de Barcelona, Departament d'Estratigrafia, Paleontologia i Geociencies Marines, Facultat de Geologia, C/Martí Franques s/n, 08028 Barcelona, Spain
[p] The Environment Institute and School of Earth and Environmental Sciences, University of Adelaide, 5005 Adelaide, SA, Australia
[q] The Institute for Photonics and Advanced Sensing (IPAS), School of Physical Sciences, University of Adelaide, 5005 Adelaide, SA, Australia
[r] Dept. Archaeology, University of Southampton, Highfield Road, Southampton, SO17 1BF, UK
[s] ICAC, Institut Català d'Arqueologia Clàssica, Plaça Rovellat s/n, 43003 Tarragona, Spain
[t] Laboratorio de Antropología Física, Facultad de Medicina, Universidad de Granada, Av. de Madrid, 11, 18012 Granada, Spain

ARTICLE INFO

Article history:
Received 4 November 2014
Received in revised form
16 February 2015
Accepted 17 February 2015
Available online

Keywords:
Upper Pleistocene
Cova del Rinoceront

ABSTRACT

The Cova del Rinoceront, a site in NE Iberia, contains a thick sedimentary fill preserving a faunal archive from the penultimate glacial and the the last interglacial periods. Layers I to III have been dated to between 74 and 147 ka, coinciding with MIS 5a to 5e, a period poorly represented in the Mediterranean terrestrial record. The results from Cova del Rinoceront are of broader interest for the reconstruction of ecological dynamics during warm stages and the understanding of the evolution and geographical variation of several taxa. The palaeoecological evidence suggests a landscape dominated by mixed wooded vegetation with mild climatic conditions, slightly more humid than today. Several vertebrate taxa, including *Haploidoceros mediterraneus*, *Stephanorhinus hundsheimensis* and *Glis glis*, are documented for the first time in the early Upper Pleistocene of Europe, showing that these species persisted across the

* Corresponding author. GRQ, Grup de Recerca del Quaternari, SERP, Dept. Prehistòria, H. Antiga i Arqueologia, Facultat de Geografia i Història, Universitat de Barcelona, C/Montalegre, 6, 08001 Barcelona, Spain.
E-mail address: jdaura_lujan@ub.edu (J. Daura).

http://dx.doi.org/10.1016/j.quascirev.2015.02.014

MIS 5
Multiproxy data
Iberian Peninsula
Palaeoenvironment

region for longer than previously thought. In addition, the recovery of a small lithic assemblage indicates human presence in the surroundings of the site. The 11 m-thick stratigraphic section also provides an ideal setting in which to compare several geochronological methods. U–Th dating of the flowstones that cap the deposit, of speleothems formed along the cave walls, and of speleothems buried by the deposit at different elevations provides minimum and maximum ages of 74 and 175 ka, respectively, for the accumulation. The ages obtained by luminescence, electron spin resonance (ESR), amino acid racemisation (AAR), palaeomagnetism and U-series dating of bone are in good agreement with each other and are stratigraphically consistent. This well-dated faunal succession presents a unique opportunity to assess changes in the Pleistocene fauna of the Mediterranean coast over an interval of more than 100 ka.

1. Introduction

It is generally understood that the Eemian interglacial, first described by Harting (1852) and commonly used by palaeontologists to define faunal and vegetal assemblages, corresponds to parts of marine and ice core records dated to MIS 5 (Shackleton et al., 2003). High resolution analyses of these cores (Sánchez-Goñi et al., 1999, 2012, 2013) demonstrate the existence of warm climate conditions, and studies of speleothems have been used to reconstruct terrestrial responses to climate change during this period (Plagnes et al., 2002; Hodge et al., 2008; Wainer et al., 2011).

Last Interglacial palaeoecological evidence from terrestrial records is typically imprecise and fragmentary due to the absence of long stratigraphic sequences. Archaeological and palaeontological studies carried out in central Europe (Kolfschoten, 2000), southeast France (Crégut-Bonnoure et al., 2010) and Britain (Currant and Jacobi, 2001) provide recent information, while cave speleothems have been used to reconstruct the climate during this period in the Mediterranean (Bar-Matthews, 2003; Muñoz-García et al., 2007).

Below latitude 41°, however, biotic records are poor, particularly in the Iberian Peninsula. Cueva del Camino in Central Iberia (Arsuaga et al., 2012; Blain et al., 2014) and Lezetxiki in the Cantabrian Range (Falguères et al., 2005) date to this time period but, given their geographical location (Cueva del Camino is situated in the northern Meseta at ~1114 m amsl and Lezetxiki is in the bioclimatic Eurosiberian region), the palaeoclimatic and environmental parameters derived from these records cannot be extrapolated to Mediterranean areas. Here, the data are scant and from only a few localities – namely, Cova de Bolomor and Cova Negra in the País Valencià (Blasco et al., 2008; Fernández Peris et al., 2008), and Teixoneres (Rosell et al., 2010) in Catalonia. Palaeobotanical reconstructions derived from pollen sequences exist for a few lacustrine and caves sequences, namely Padul and La Carihuela, respectively (González-Sampériz et al., 2010, 2013; Carrión, 2012). Anthracological data are also available for Abric del Pastor (Vidal-Matutano, 2015), where, however, the data are insufficient to warrant secure chronological assignment to the Last Interglacial.

Europe's Late Pleistocene large mammal record is characterised by the cool-adapted *Coelodonta-Mammuthus* faunal complex (Kahlke, 1999; Stuart et al., 2002; Barnosky et al., 2004; Stuart, 2005; Kahlke et al., 2011). In the Iberian Peninsula, this faunal complex is the result of successive expansions of steppe landscapes from Central Europe. Although cold-adapted species have been observed in Iberia during MIS 6 (Álvarez-Lao, 2007), it was not until MIS 4/MIS 3 that such expansions were widespread. On closer inspection, the northeast Iberian record (Álvarez-Lao, 2007) reveals that cold-adapted taxa, such as woolly rhinoceros (*Coeleodonta antiquitatis*) and woolly mammoth (*Mammuthus primigenius*), are poorly documented, as are arid and open environment species, such as *Equus hydruntinus* (Burke et al., 2003; Orlando et al., 2006); the same applies to other large mammals that could be considered cold climate indicators at this latitude (Daura et al., 2013). This expansion of cold-adapted taxa and attendant faunal renewal conceivably occurred around the Last Interglacial–Last Glacial transition (MIS 5a/MIS 4), with the eventual disappearance of species adapted to warmer climatic conditions.

The ability to test hypotheses about palaeoenvironmental and biotic changes across the Iberian Peninsula is limited by the absence of reliable chronologies beyond the limits of radiocarbon dating. Cova de Bolomor's stratigraphic sequence is thought to span the MIS 9-MIS 5e (~500–100 ka) interval (Fernández-Peris, 2007), based on Thermoluminescence (TL), aminoacid racemisation (AAR) and magnetosusceptibility (MS) results, with a single TL age of 121 ± 18 ka on sediments from layer II, which caps the Pleistocene sequence. The results range from 55 to 350 ka (Falguères et al., 2005), but the different dating techniques (ESR, U–Th and ^{14}C) applied to this site reveal a number of contradictions. Other Iberian sites have been dated with even less certainty as results are based on one geochronological method only. For example, the age of the Cueva del Camino deposit has been constrained using multi-grain optically stimulated luminescence (OSL) dating, which yielded an MIS 5 chronology (Arsuaga et al., 2012); however, as argued by Álvarez-Lao et al. (2013), these OSL ages are not precise enough to differentiate between sub-stages of MIS 5. Elsewhere, a flowstone dated to between 100 and 94 ka provides a maximum age for layer III of Teixoneres Cave (Rosell et al., 2010; López-García et al., 2012).

As karst entry points are natural traps for biota and sediments, the debris cones formed via openings in cave roofs contain abundant fossil remains related to the exterior environment. In addition, these deposits are occasionally sealed by speleothems, which can be dated using uranium disequilibrium series methods and other geochronological techniques applicable to faunal remains and sedimentary fills. This paper presents a study of the Cova del Rinoceront site, a palaeontological archive located in the Mediterranean coast of NE Iberia containing one of the region's longest MIS 5 stratigraphic sequences. Fossil vertebrate remains are abundant and provide important data for palaeoenvironmental reconstructions of the northernmost mesomediterranean area (Rivas-Martínez, 1987) prior to the onset of the Last Glacial period.

2. General setting and site description

Cova del Rinoceront (41°16′24.92″N, 1°57′39.18″E, 25 m amsl) is located in the eastern Garraf Massif (<600 m high), in the Can'-Aymerich quarry, municipality of Castelldefels (20 km to the southwest of Barcelona). The cave formed in a fractured narrow band, known as the La Ginesta fault, that runs in NE–SW direction over 2 km (Fig. 1-1). The original morphology of the site is unknown, as a significant part of it was destroyed in the 1960s by quarrying (Fig. 1-3), which exposed the sedimentary fill along a vertical S–N trending section (Fig. 1-2). The original entrance would probably have been a now lost shaft connecting the extant

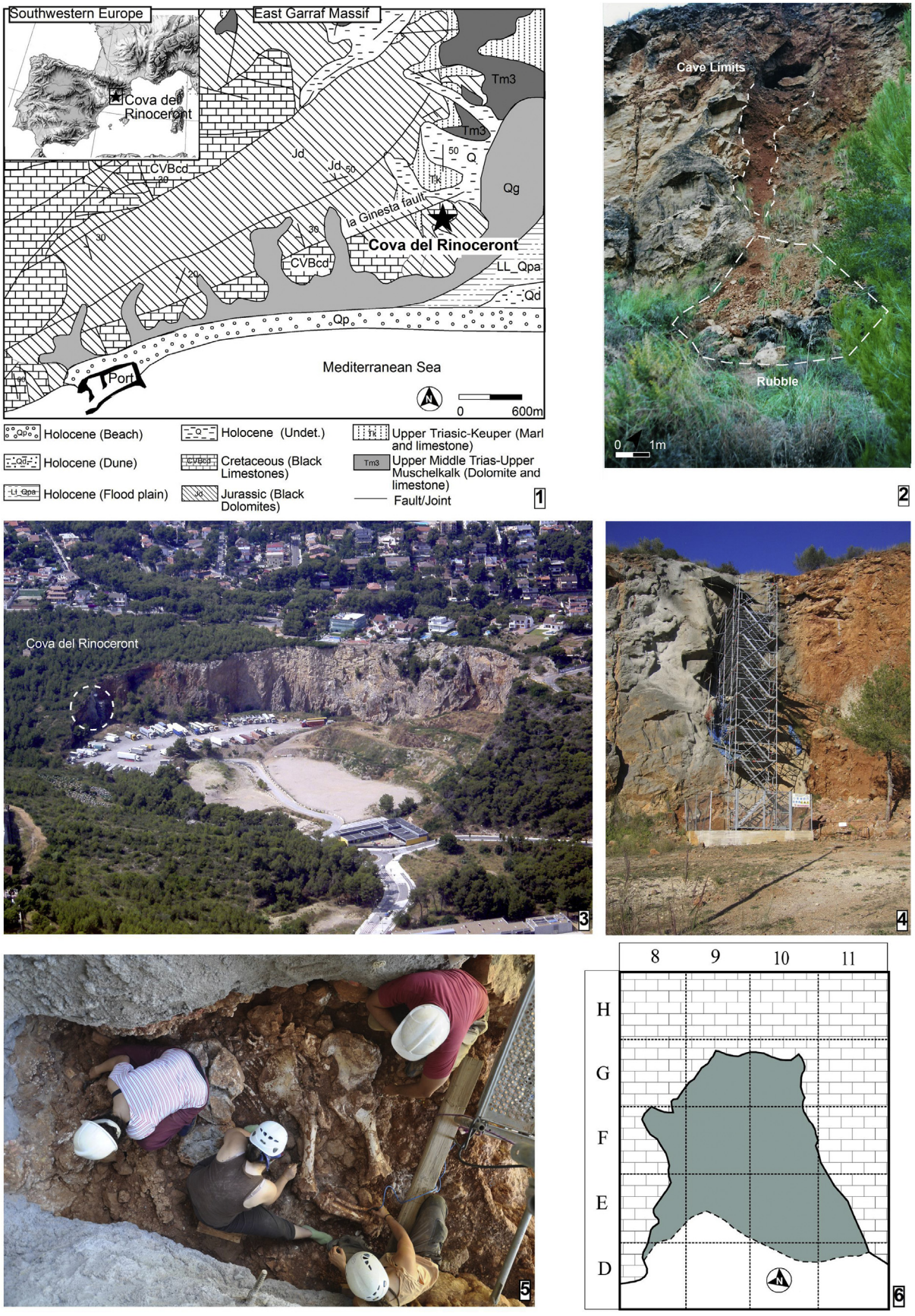

Fig. 1. Cova del Rinoceront site. 1: Location with basic regional geology. 2: ca n'Aymerich quarry and Cova del Rinoceront (circle). 3: Plan of the site. 4: The site before restoration. 5: Cova del Rinoceront after restoration with scaffold access. 6: Layer III excavation area.

part of the site with the surface, 6 m above. Shafts and sinkholes are one of the most frequent features characterising the karst landscape of the Garraf massif (Daura et al., 2014). The exposed stratigraphy consists of breccias formed by degradation of wall and roof material, and contains vertebrate remains; a few stone tools have also been recovered. The metre-to-centimetre-sized angular clast component of these breccias is more abundant and coarser towards the north wall, suggesting that the karst opening was located close to this area. The predominant facies consists of a coarse-grained and clast-supported limestone breccia with a calcite-cemented red silty sand matrix. The matrix derives from host rock impurities and from the sediment cover of the exokarst. As a result of these formation processes, the blocks display a chaotic orientation and a random distribution.

Although, in the past, Pleistocene fossils had been described from the same general area (Almera, 1898; Villalta and Crusafont, 1950; Vicente, 1965), it was not until 2002 that Cova del Rinoceront was discovered (Daura et al., 2005, 2010). Prior to excavation, a clearing and sieving campaign was conducted on the rubble accumulated at the foot of the quarried face of the cave, and rehabilitation work was undertaken at the site to guarantee the preservation of the deposit and the safety of fieldwork conditions (Sanz et al., 2011). In order to access the site, a 20 m-high scaffolding tower had to be erected (Fig. 1-4). The ten excavation campaigns (Fig. 1-5) conducted at the site by the Grup de Recerca del Quaternari (GRQ) have documented a stratigraphic sequence exposed over a depth of 11 m and a width of 3 m (Fig. 1-6). The sequence can be divided into three main units, comprising eight layers designated I to VIII (from top to bottom).

3. Materials and methods

3.1. Excavation methodology

The rubble accumulated at the base of the quarry face (Fig. 1-2) equated to about 60 m^3 of debris, which was sieved with meshes of 10, 6, 3, 1.4 and 0.4 mm; this reworked material derives mainly from layers I, III, and VI.

Archaeological work to date, herein presented, has focused on describing and sampling the stratigraphic profile, sieving the fallen sediments accumulated at the foot of the section, and excavating layers I to III; we have also carried out a test pit into layers VI to VIII.

Excavation was carried out using standard archaeological and palaeontological techniques, with three-dimensional plotting of finds. Stone tools, large mammal bones, tortoise carapaces, lagomorph cranial remains and charcoal fragments were mapped in situ prior to removal, while land snail shells and lagomorph postcrania were bagged by 1 m^2 units of provenience. Sediments were dry-sieved using superimposed 5 and 1 mm mesh screens. Recovery of the micromammal remains and other small bones was effected via wet-sieving of the 2.0–0.4 mm fraction at the archaeological laboratory (La Guixera) maintained by the Castelldefels Town Council.

The palaeontological remains from layers I to III were partially encased in hard calcareous breccias that had to be excavated with pneumatic microhammers and microchisel (Mod. CTS 178). Fossils were restored using normal air scribe (Mod. W 224), and consolidated with Paraloïd-B72 dissolved with acetone. Restoration was carried out in the La Guixera laboratory.

3.2. Sampling and laboratory methods

3.2.1. Sedimentology

Stratigraphic description and sample collection focused on the main vertical profile. After air-drying for 24 h, a total of 8 samples from layers I to VIII were colour-described (dry and humid) using the MUNSELL© soil colour chart, and then subjected to grain-size and mineralogical analyses. Particle size distributions were determined using a Beckman Coulter-LS™ particle size analyser. Cumulative curves, frequency histograms and summary statistics were calculated from these datasets.

Mineralogy was determined with a Siemens© D-5000 X-ray diffractometer, using randomly oriented powder from the bulk samples. Samples were pre-treated with H_2O_2 to remove organic matter. Replicates were heated to 375 or 600 °C for 1 h or treated with ethylene glycol at 60 °C to differentiate between clay minerals. Selected samples were analysed by EDX (Bruker© X-Falsh Detector 4020) or observed by SEM (Hitachi© S-3400N). Semi-quantitative mineral analyses were based on the peak areas obtained using EVA© ver. 7.0 software.

3.2.2. Speleothem dating

Several dating methods have been used to establish a chronological framework for the site. Speleothem dating was carried out using the U-series disequilibrium method (Ivanovich and Harmon, 1992) at the Institute of Earth Sciences "Jaume Almera" (Barcelona). In cave environments, water-soluble uranium isotopes co-precipitate at the time of calcite deposition and generally behave as a closed system. Numerical ages are calculated directly from the daughter/parent ratio of $^{230}Th/^{234}U$, assuming that all the measured ^{230}Th was formed by in situ decay of the ^{234}U and ^{238}U originally present. Additional detrital ^{230}Th could have been supplied by clays that were mechanically mixed-in with the carbonate precipitates. However, these clays also harbour large amounts of ^{232}Th (common) thorium, which is not part of the $^{238}U–^{234}U$ decay series; hence, the $^{230}Th/^{232}Th$ activity ratio can be used as an indicator of the degree of contamination.

The procedure used for chemical separation was based on Bischoff and Fitzpatrick (1991): samples were totally dissolved in strong mineral acids and an artificial radioisotope with known activity was incorporated into the solution to determine the efficiency of the isotope separation. The U and Th isotopes were isolated by ion-exchange chromatography and then analysed in an alpha spectrometer from Ortec with a silica barrier detector. The program UDATE from Rosenbauer (1991) was used for age calculation.

3.2.3. U-series dating of teeth and bone

A fossil tooth was directly dated at the University of New Mexico by U-series analysis. The U–Th separation chemistry used in this study has been described previously in Asmerom et al. (2010). The piece of tooth was dissolved in aqua regia, then spiked with a mixed solution of ^{229}Th, ^{233}U, and ^{236}U, and fluxed at moderate heat for 1 h. It was dried down, treated in 7 M nitric acid, and loaded into columns. U and Th were separated using Eichrom 1 × 8, 200–400 mesh chloride from anion exchange resin. The U and Th fractions were loaded in 3% nitric acid and analysed on a Thermo Neptune multi-collector inductively coupled plasma mass spectrometer (MC-ICP-MS). Standards NBL-112, and an in-house $^{230}Th–^{229}Th$ solution were analysed during the run sessions. We have used improved radioactive half-lives for ^{230}Th and ^{234}U, and a modification of the analytical methods for MC-ICP-MS following Cheng et al. (2013). U-series age corrections were based on an initial $^{230}Th/^{232}Th$ atomic ratio of 4.4 ± 2.2 ppm.

Two bone samples were dated at the University of Bristol. U–Th ratios were measured across two transverse bone sections by laser ablation on a Thermo Fisher Neptune MC-ICP-MS using the method outlined in Pike et al. (2005). Uranium uptake in the bone was interpreted on the basis of distributions of U and U-series isotopes according to the diffusion-adsorption model (Pike et al., 2002).

Apparent closed system dates were calculated using the U and Th isotopes integrated across the bone section, using decay constants and uncertainties given in Cheng et al. (2013).

3.2.4. AAR dating of shell

The amino acid epimerisation/racemisation analyses were performed in the Biomolecular Stratigraphy Laboratory (Madrid, Spain) using the following techniques: 1) gas chromatography (GC) with a nitrogen/phosphorous detector for samples #35 to #37 and #39 to #41 and; 2) reverse phase high-performance liquid chromatography (HPLC) for samples #28, #33 and #34.

Peripheral parts of *Testacella haliotidea* opercula (approximately 20–30%) were removed after chemical etching with 2M HCl. Afterwards they were carefully cleaned by sonication in distilled deionised (DDI) water and rinsed with DDI water to remove sediment.

The amino acid preparation protocol for GC analysis is described in Goodfriend (1991) and Goodfriend and Meyer (1991). Samples were injected into a Hewlett–Packard 5890 gas chromatograph with an NPD detector equipped with a Chirasil-L-Val-fused silica column (0.39 mm × 0.25 μm × 25 m) from Chrompack. The NPD detector was set at 300 °C.

Amino acid concentrations and D/L values were quantified by high performance liquid chromatography (HPLC) following the sample preparation protocol described by Kaufman and Manley (1998) and Kaufman (2000). Samples were injected into an Agilent-1100 HPLC equipped with a fluorescence detector. Excitation and emission wavelengths were programmed at 335 nm and 445 nm, respectively. A Hypersil BDS C18 reverse-phase column (5 μm; 250 × 4 mm i.d.) was used for the separation.

As we regularly analyse amino acid standards of all enantiomers (Sigma) and those from the inter-laboratory comparison (ILC) of Wehmiller (1984), the total concentration of the amino acids in the samples determined by GC was obtained from comparison with the peak area of the analysed standards. For samples analysed by HPLC, we also used an internal standard (L-*homo*-arginine).

3.2.5. ESR dating of teeth

Electron spin resonance (ESR) dating is one of the family of 'trapped charge' dating methods that also includes TL and OSL. For a general review see Rink (1997). The dated tooth was collected in 2008 from sub-layer IIc (grid unit G8) and corresponds to a deer tooth classified as *Haploidoceros mediterraneus*.

The enamel was mechanically separated from the dentine for ESR measurements. After removing 20 μm from each side to eliminate effects of α-radiation, the enamel was powdered to a range of 90–150 μm and divided into aliquots of approximately 20 mg each. Using a ^{60}CO γ source, all but one of the aliquots were irradiated at a dose rate of 56–132 Gy/s with added doses ranged from 10 to 2200 Gy. ESR spectra were measured with a JEOL RE1X spectrometer at 25 °C, using 2 mW power under a 100 KHz field modulation, and a 0.3 s time constant. The spectra were scanned over 10 mT, centred at 336 mT with an 8.0 min sweep time. Gains were set to maximise signal intensity.

3.2.6. Luminescence dating of sediments

Seven sediment samples were dated using multi-grain aliquot infrared stimulated luminescence (IRSL) and TL at the Laboratorio de Datación y Radioquímica-Universidad Autónoma de Madrid. Samples were collected from freshly cleaned sections of layers I, II, III, V and VI using plastic tubes and wrapped in light-proof bags for transportation. Sampling focused on the most homogeneous sedimentary layers (avoiding proximity to large clasts) and targeted horizons that contained sufficient amounts of silt-sized silicate minerals. After transferring the luminescence dating samples to safe-light laboratories, the fine-grained (2–10 μm) polymineral fractions were prepared for burial dose estimation using standard procedures (Aitken, 1998).

The IRSL and TL measurements were made using a Risø TL-DA-10 reader equipped with IR LEDs, a heater plate and a calibrated ^{90}Sr/^{90}Y beta source. Polymineral fine-grain equivalent dose (D_e) estimates were determined from ultraviolet emissions using a multiple aliquot additive dose (MAAD) protocol. Preheats of 180 °C for 10 s and 90 °C for 120 s were used prior to IRSL and TL stimulations, respectively. Plateau tests were used to isolate the thermally stable region of the TL glow curve for D_e integration (320–370 °C for sample #24; 350–400 °C for sample #25). Environmental dose rates were calculated on dried and homogenised, bulk sediment samples using a combination of beta counting and thick-source alpha counting. Cosmic-ray dose rate contributions were calculated from high energy gamma emissions recorded in situ using a NaI(TL) gamma spectrometer. For alpha dose rate calculations, alpha effectiveness (*a*-value) was determined on a sample-by-sample basis by comparing IRSL or TL signals induced by 3.7 MeV alpha particles (using a ^{241}Am source) with corresponding signals induced by beta irradiation (using the ^{90}Sr/^{90}Y source) (Zimmerman, 1971). The conversion factors of Nambi and Aitken (1986) were used to derive dose rate estimates from measured elemental concentrations and specific activities. The final dose rates have also been adjusted for water attenuation effects (Aitken, 1985), using present-day sediment moisture contents.

3.2.7. Magnetostratigraphy

The sedimentary infill of the cave was sampled for magnetostratigraphy. Because coarsely grained sediments are unsuitable for palaeomagnetic studies, only a few samples could be obtained from a limited number of red clay layers. Oriented rock blocks were drilled in the laboratory and shaped to standard palaeomagnetic samples of 10.4 cm^3. Samples were stepwise demagnetised at temperature intervals of 50 °C up to 500 °C and, above this temperature, at closer steps up to complete demagnetisation. A high proportion (75%) of the Natural Remanent Magnetisation (NRM) was demagnetised at temperatures under 250 °C, this interval defining a low-temperature viscous component which is subparallel to the drilling direction. The remaining magnetisation defines a characteristic NRM component with maximum unblocking temperatures ranging between 550 °C and 600°, and possibly having magnetite as the principal remanence carrier.

3.2.8. Palaeontology

A range of bioarchaeological methods have been used to reconstruct the palaeoenvironmental conditions of the site. A taxonomic study of faunal remains was accomplished using several classic palaeontological methods. For large mammals, taxonomic assignments and a preliminary Minimum Number of Individuals (MNI) index have been established from the restored material; skeletal part counting is still in progress. Micromammal and bird bone remains were subjected to the same taxonomic studies; given the small size of these samples, it has already been possible to calculate MNI and Number of Identified Specimens (NISP) for each taxon.

3.2.9. Phytoliths

A total of 13 samples from sediments and dental calculus were analysed for phytoliths and starch content. The tooth come from different individuals of *Haploidoceros mediterraneus* and single specimens of *Capra* cf. *ibex*, *Cervus elaphus* and *Stephanorhinus hundsheimensis*. All of these individuals came from layer I, with the exception of the rhinoceros sample, which was recovered from the rubble and has been ascribed to layer III. Samples were collected

from the molars and premolars, which are used for chewing and retain a greater number of microfossils (Boyadjian et al., 2007). *C. elaphus* had a considerable amount of calculus and thus the phytolith extraction was divided into three samples, one premolar and two molars (P_3, M_1, M_3). For comparative purposes, two sediment samples were collected close to this *C. elaphus* individual as well as from layer I.

The phytolith and starch extraction from dental calculus followed Middleton and Rovner (1994). Calculus was collected with a dental scaler and treated with 1N HCl to eliminate carbonates. As phytoliths were still embedded in the calculus, the *C. elaphus* M_1 and M_3 were treated a second time with 6N HCl. The phytolith extraction from sediment samples followed Albert et al. (1999). Carbonates, phosphates and organic material were dissolved using 3N HCl, 3N HNO_3 and hydrogen peroxide (H_2O_2). The remaining sample was then density-separated by adding 5 ml of sodium polytungstate. Phytoliths and starches were identified using an Olympus BX41 petrographic microscope. The morphological identification of phytoliths followed Albert et al. (2011) as well as standard literature. Phytoliths and starches were described following the International Code Nomenclatures for Phytolith (ICPN) (Madella et al., 2005) and Starches (ICSN, 2011).

3.2.10. Wood charcoal

The analysis of the charcoal assemblage was carried out using a reflected light optical microscope (Olympus BX41). In order to identify the charcoal fragments, we examined three anatomical sections of each specimen (transverse, longitudinal tangential, longitudinal radial).

4. Results

4.1. Stratigraphy

Eight layers have been identified in the 11 m-thick sequence (Fig. 2). Layers I, II and III were completely excavated between 2003 and 2012. At this elevation, the deposits fill an area of about 6 m^2 (length, 2 m; maximum width, 3 m).

The cave sediments are mainly composed of rock fragments in a clast-supported or matrix-supported fabric but gravels, sands, silt and clay can be readily distinguished in the lower layers (VIII, VII and VI). Significant carbonate cementation is apparent in the upper part of the sequence, while the basal layers (VI, VII and VIII) are either non-cemented or poorly cemented. From a petrological point of view, three different elements can be distinguished; (i) calcareous clastic rocks that are derived from the host bedrock, (ii) a matrix composed of reddish clay and silty-clay developed from the insoluble residues of limestone (*terra rossa*), although an allochthonous aeolian component cannot be excluded; and (iii) a calcite cement resulting from the percolation of water saturated with calcium carbonate.

The excavation of layers I to III revealed a preferential clast orientation of 170–210° and a dip of about 18–20°. However, to date, we have not been able to recognise any distinguishing solifluction lobes or debris-flow structures. The large-sized blocks probably accumulated from the collapse of the cave walls and roof. The diameters of these blocks range from centimetres (>20 cm) to more than 1.5 m, resulting in a chaotic clast-supported breccia. The smaller sized component of the breccias (<10 cm) may be derived from the La Ginesta fault and accumulated by occasional rainfall-triggered, debris flow events.

The eight sedimentary layers have been grouped into three lithological units on the basis of stratigraphic unconformities, clast size, matrix abundance and cement content (Table 1 and Fig. 2). Unit 3, the lowermost unit, comprises clay and silt layers VIII and VI and intervening layer VII, which is mainly composed of slightly upward-coarsening gravels. The lack of archaeological and palaeontological remains in layer VIII and part of VII suggests that, at the time of their formation, no connection with the exterior existed yet. These layers may represent a backswamp facies (Bosch and White, 2004) made up of weathered bedrock residue and fine material from exterior soils infiltrated through small fissures.

Unit 2 is the middle unit and comprises layers V and IV. Layer V is composed of limestone clasts, which are either unweathered roof-fall blocks (some of which are very large) or weathered blocks sourced from the cave exterior. Layer IV is composed of gravels and granules, and is devoid of a finer matrix. The sedimentary characteristics of these layers imply open conditions and the prevalence of a dry climate. The boundary between Units 2 and 1 is abrupt and represents a shift in sedimentary dynamics.

The deposits of Unit 1 are oriented to the west and can be differentiated into three alternate clast-supported depositional episodes (layers I, II, III). These sediments are composed of sub-rounded gravels (50–30%), sands and clays. Several different sub-layers have been identified within layers I, II and III, as detailed in Fig. 2 and Table 1.

4.2. Dating evidence

In total, 47 samples were collected from the excavation and the vertical cutting as part of our multi-technique dating study (Fig. 2). Of these samples, 17 (#1 to #17) were collected for U–Th dating, from the flowstone capping the top of the stratigraphic profile and from various types of cave speleothems; 1 tooth (#18) and 2 bone samples (#19 and #20) were taken for U–Th dating; 7 (#21 to #27) were taken for luminescence dating; 15 gastropod opercula (#28 to #42) were dated using amino acid racemisation; 1 tooth enamel sample (#43) was processed for ESR dating; and 4 samples (#44 to #47) were collected for palaeomagnetism.

4.2.1. U–Th dating

In a limestone massif such as the Garraf, located close to the sea and with the base of the karst situated below sea level, the karst system is characterised by the influence of geomorphic processes such as soil weathering, flowstone precipitation, limestone erosion and debris cone accumulation, operating over geological time scales. The relationship between environmental processes and debris cone formation has been used previously to establish mid-Pleistocene palaeoclimate models from preserved fossil remains and U–Th chronologies (Moriarty et al., 2000; Hearty et al., 2004; Daura et al., 2014). Of the 17 samples analysed for U–Th dating at Cova del Rinoceront, seven did not contain ^{232}Th and were considered reliable for dating, six were slightly contaminated ($^{239}Th/^{232}Th$ value >15), and the remaining six were significantly contaminated by ^{232}Th. The three samples (#1, #2 and #3) from the capping flowstone (i.e., the speleothem that seals the entire debris cone deposit) provide the youngest (*ante quem*) ages for the sequence. Two samples (#4 and #5) were collected from the calcite coating of fissures in layer III and provide a minimum age for this unit, seven come from the cave walls, from wall-perched stalactites or from stalactites covered by sediments from layers I to VII (#6 to #14), and three are from sparry calcite cements on cave wall covered by layers VII and VIII (#15 to #17) (Table 2).

From the point of view of their purity and measured ages, the speleothem results obtained can be grouped into four categories and reveal four vadose phases:

- Group 1 includes samples #15, #16 and #17, which were taken from sparry calcite (dog-tooth spar) located at the base of the karstic conduit under the fill of layers VIII–VII, between sediment and bedrock, as well as sample #8, which is a sparry calcite

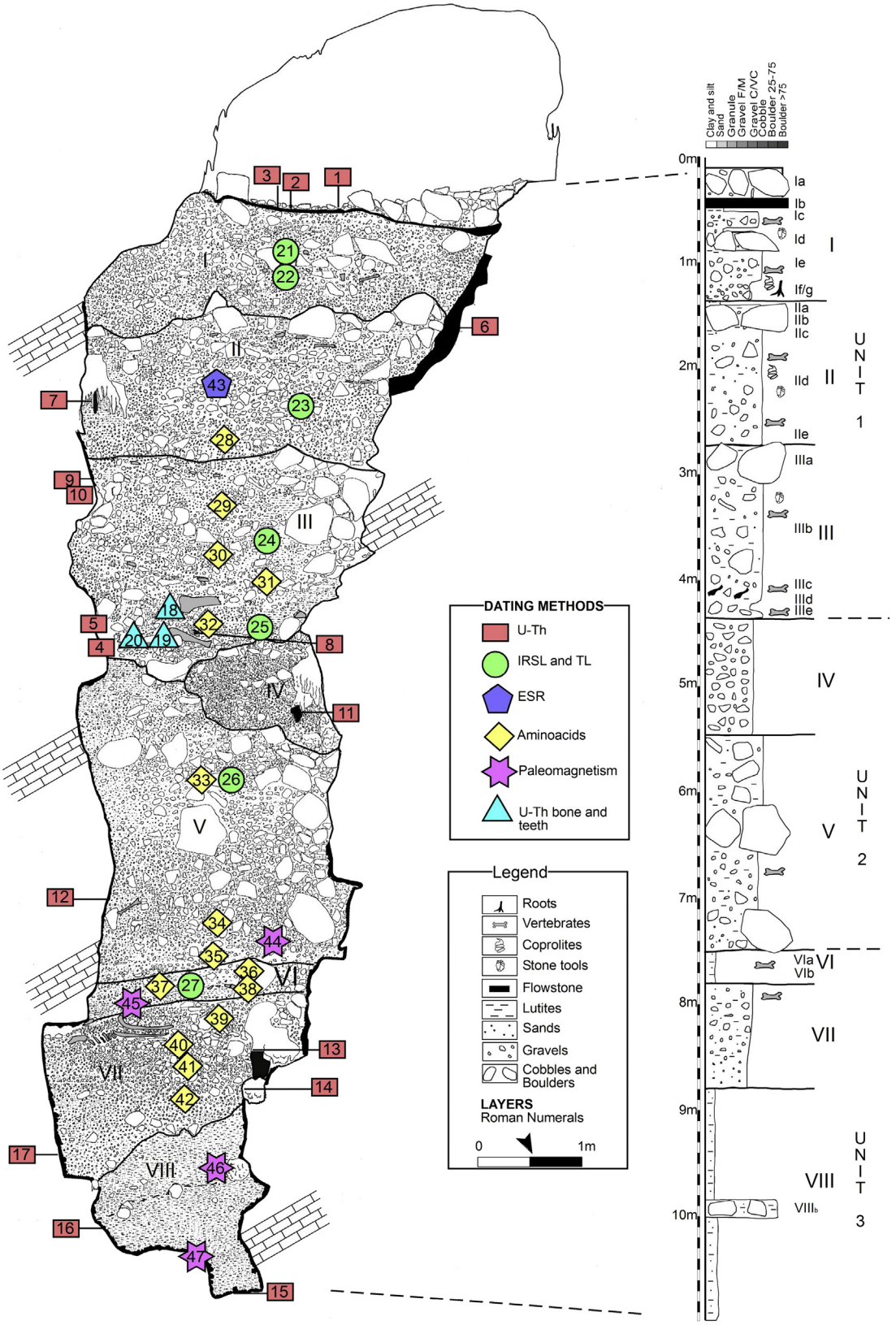

Fig. 2. Stratigraphic profile of Cova del Rinoceront.

(dog-tooth spar) clast in layer III that has fallen from the roof or wall; these samples were impossible to date because the speleothems are at isotopic U/Th equilibrium, yielding a (conservative) minimum age of 350 ka.

- Group 2 contains stalagmites #7 and #11 and the lateral flowstone 6; these samples are less contaminated and the nominal ages range between ~218 and ~261 ka, giving an average of ~234 ka for one of the cave ornamentation phases;

Table 1
Main layers identified and stratigraphic description of Cova del Rinoceront.

Unit	Layer	Description
3	VIII	**Silt and clay**. Located at the base of the cave, and consisting of silts and clays with rare occurrences of cobbles (VIIIb) (backswamp facies). An increase of gravels occurs towards the top; colour red 2.5YR 4/6; thickness ~150 cm; 970/1120 cm depth below datum. Clay mineralogy: Smectite/Montmorillonite 2.2%; Muscovite/Illite 3.6%; Kaolinite 1.2%; Quartz 84.9%; Feldspar 5.2%; Calcite HMC 2.9%. Gran size: Clay 89.7%; Silt 10.3%.Organic matter: 2.98%.
	VII	**Clast-supported breccia**. Located above layer VIII and consisting of coarsening upward accumulations of subangular clasts. Boulders are present at the base and are surrounded by a lutitic matrix with gravels; colour red 5YR 4/6; thickness ~150 cm, 850/970 cm below datum. Clay mineralogy: Muscovite/Illite 2.8%; Kaolinite 1.4%; Quartz 52.7%; Feldspar 4.8%; Calcite HMC 38.4%. Gran Size: Clay 15.4%; Silt 14.2%; Granule and Sands 26.3%; Gravels, Cobbles and Boulders 44.2%. Organic matter: 3.8%.
	VI	**Clay and Silt**. This layer shows an increase in boulder content and a silty-sandy matrix that bears iron oxides. This layer is similar to layer VIII and could be interpreted as a backswamp facies or as indicating the existence of a restricted entrance. It shows variations in texture and grain size that permit the discrimination of sublayers VIa from bottom; colour red 2.5 YR 4/6; thickness ~60 cm, 800/850 cm below datum. Clay mineralogy: Muscovite/Illite 2.4%; Kaolinite 1.8%; Quartz 81.7%; Feldspar 4.3%; Calcite HMC 9.7%. Gran Size: Clay 85.3%; Silt 13.9%; Granule and Sands 0.8%. Organic matter: 4.2%.
2	V	**Mud supported breccia**. Corresponds to a thick layer, which is very heterogeneous and contains large size boulders with subangular morphology and a sandy-silty matrix. Boulder accumulations are found mostly in the eastern part of the cave, with matrix dominating on the western side (V_2); colour: red 2.5 YR 4/6; thickness ~250 cm tick, 565/800 cm, below datum. Clay mineralogy: Muscovite/Illite 1.6%; Kaolinite 1.7%; Quartz 61.7%; Calcite HMC 35.1%. Gran Size V and V_2 respectively: Clay 19.8–36.2%; Silt 10.7–25.9%; Granule and Sands 19.6–19.3%; Gravels, Cobbles and Boulders 49.9–18.5%. Organic matter: 4.7%.
	IV	**Clast supported breccia**. Consists of subangular coarse and very coarse clasts alternating with boulders in scarce matrix; colour dark reddish brown 2.5YR; thickness ~80 cm; 525/565 cm below datum. Clay mineralogy: Muscovite/Illite 1%–1.7%; Kaolinite 0.8%–2.2%; Quartz 62.5%–64.5%; Feldspar 0.5%–0%; Calcite HMC 35.2%–31.6%. Gran Size: Clay 4.3%; Silt 3.2%; Granule and Sands 15.5%; Gravels, Cobbles with minor Boulders 76.8%. Organic matter: 4.6%.
1	III	**Clast supported breccia**. Large size subangular boulders and gravels surrounded by a weakened red sandy-silty matrix. Texture is very similar throughout the layer, though different fossil horizons can be distinguished: the first one (sub-layer IIIe) is found in the lower part containing *S. hundsheimensis*; another one is located immediately above, and separated by a crust (IIId) with Proboscidian remains (IIIc) and; the uppermost fossil horizon contains *Testudo hermanni* (IIIb) with large blocks (IIIa); colour dark reddish brown 5YR 3/4, thickness 220 cm, 330/525 cm below datum. Clay mineralogy IIIc/d/e and IIIa/b respectively: Muscovite/Illite 1.7%–1.2%; Kaolinite 2.2%–1.4%; Quartz 63.6%–31.9%; Feldspar 0.7%–1.4%; Calcite HMC 31.9%–63.3%; Dolomite 0%–0.7%. Gran Size IIIbase and III respectively: Clay 11.8% –13.6%; Silt 12.5%–12.9%; Granule and Sands 20.8%-22.9 %; Gravels, Cobbles and Boulders 54.9%–50.6%. Organic matter: 5.6%.
	II	**Clast supported breccia**. This layer represents a poorly cemented breccia and is composed of large size boulders (60–150 cm), gravels and a sandy–silt matrix. Its lower limit is defined by the presence of large fallen boulders accumulated along the western side (IIIa). Variations in grain size are noticeable (IIa to IIe). Colour: yellowish red 5YR 5/8; 120 cm tick, 226/330 cm below datum. Clay mineralogy sub-layer IIc and IIa/b respectively: Muscovite/Illite 2.7%–2.7%; Kaolinite 2.3%–1.5%; Quartz 62.9%–70.6%; Feldspar 0%–3.3%; Calcite HMC 30.6%–22%. Gran Size: Clay 16.1%; Silt 16.0%; Granule and Sands 20.0%; Gravels, Cobbles and Boulders 47.9%. Organic matter: 5.2%.
	I	**Clast supported breccia**. This layer is located beneath the flowstone and corresponds to the uppermost Pleistocene layer. Formed by subangular large-sized boulders, which are surrounded by a sand-silty matrix and are poorly cemented. The lower limit is an accumulation of limestone blocks (IIa) with a concave disposition and slight slope towards the SE. Variations in gran size and boulder accumulations are noticeable: sub-layer Ig is composed of sub-angular gravels without matrix, sub-layer If is a rhizoconcretions horizon, sub-layer Ie is a clast unit, sub-layer Id corresponds to large blocks and sub-layer Ic is characterised by the dominance of clasts. Colour: ranges from dark red 10R3/6 to reddish yellow 7.5YR 7/6; thickness 150 cm; 100/226 cm below datum. Clay mineralogy: Smectite/Montmorillonite 2.5%; Kaolinite 2.1%; Quartz 73.7%; Feldspar 6.7%; Calcite HMC 15%. Gran Size: Clay 22.2%; Silt 17.5%; Granule and Sands 23.9%; Gravels, Cobbles and Boulders 36.4%. Organic matter: 4.4%.
	Ib	**Flowstone**. The sequence ends with a characteristic cave flowstone displaying different degrees of crystallinity and purity. In some areas the lower part the flowstone contains cemented bones and sediment infill from layer I. Above this layer, rubble has accumulated as a result of quarry activities (Ia).

despite its higher Th content, sample #13 can be included in this group.

- Group 3 includes samples #10, #12a and #14, which were collected from different parts of the walls of the cave and have a high degree of purity; these two samples yielded ages of between 150 and 170 ka and could correspond to a film-forming, along-the-wall, fluid circulation phase; despite its higher Th content, sample #9 can be included in this group.
- Group 4 includes the most recently formed samples from the stratigraphic profile. Two of the three samples from the capping flowstone overlying layer I (#1 and 2) are not contaminated and yield indistinguishable ages of 82.9 ka+4.7–4.6 and 83.7 + 6.0/−5.7 ka. However, the third sample (#3) exhibits a high ^{232}Th value, which is indicative of detrital contamination. Samples #4 (89.3 + 4.1/−3.9 ka) and #5 (104.4 + 8.0/−7.5), collected from calcite coatings developed in the small intervening cracks of mud-supported clasts, can also be associated with this fluid flow phase; it cannot be excluded that they formed after the cave was completely buried.

Concerning the bone and tooth U-series dates, the elephant tusk (#18) result of ~95 ka is significantly younger than the results for the rhinoceros bone samples (#19 and #20), which gave statistically consistent closed system dates of ~130 ka. However, leaching of uranium, indicated by the inverse correlation of U concentration with ^{230}Th/^{238}U was apparent towards the outer and inner surfaces of the bone sections. The leaching of uranium leads to apparent over estimated closed system dates, and therefore we should treat these two dates as maximum ages (Fig. 3).

These results place the accumulation of Units 1 and 2 firmly in the interval between ~175 and ~74 ka, and the U–Th-dated rhino bones (samples #19 and 20) give maximum ages of 133.6 and 147 ka for the accumulation of the base of layer III (sub-layer IIIe). These data suggest that the deposition of Unit 1 (layers I-III) took place during the earlier part of the Last Interglacial, broadly coinciding with sub-stages 5c to 5e of the MIS- timescale, as suggested by the composition of the faunal assemblage recovered therein (see below), even though a MIS 5a to 5b age for layers I-II cannot be excluded.

4.2.2. IRSL and TL

Table 3 (samples #21 to #27) summarises the MAAD IRSL and TL ages obtained for the seven Cova del Rinoceront samples. Burial doses were calculated from the weighted mean of ten replicate D_e estimates per sample. The final ages have been calculated by dividing the measured D_e values by their respective environmental dose rates. Multiple aliquot storage tests conducted on these samples suggest that the polymineral IRSL and TL signals may not be significantly affected by anomalous fading – signal losses were <3% for all samples following storage times of 240–600 h. Similar results have been reported for MAAD TL and IRSL signals of

Table 2
U–Th ages of speleothem (1σ confidence interval) and bone/tooth (2 σ confidence intervals) samples.

Sample ID	Layer	Site#	Material	Lab#	U ppm	Th ppm	$^{234}U/^{238}U$	$^{230}Th/^{232}Th$	$^{230}Th/^{238}U$	Age ka
Flowstone (layer Ib) capping the deposit: terminus ante quem for sub-layer Ic										
1	Ib	8029	Flowstone	2803	0.11	****	1.20 ± 0.04	****		82.9 + 4.7/-4.6
2	Ib	8030	Flowstone	104	0.15	****	1.11 ± 0.04	****		83.7 + 6.0/−5.7
3	Ib	8031	Flowstone	2403	0.18	0.09	1.14 ± 0.03	4.021 ± 0.142		93.2 + 4.3/−4.1
Calcite coatings filling fissures in Layer III: minimum age for layer III										
4	IIId	8032	Calcite coating	1305	0.12	****	1.22 ± 0.03	****		89.3 + 4.1/−3.9
5	IIId	7860	Calcite coating	1903	0.20	0.08	1.14 ± 0.04	5.523 ± 0.401		104.4 + 8.0/−7.5
U–Th tooth and bone dating from layer III										
18[a]	IIIc	7881	Tusk (Elephantidae)	–	35.91 ± 0.05	0.016.6 ± 0.5	1.310 ± 0.001	5208 ± 153	0.78642 ± 0.00206	95.3 ± 0.4
19	IIIe	8043	Mt III (*S. hundsheimensis*)	JD9			1.32133 ± 0.00041		0.95808 ± 0.00070	129.7 + 3.7/-3.4
20	IIIe	8044	Ulna (*S. hundsheimensis*)	JD33			1.5115 ± 0.0020		1.1186 ± 0.0034	131 + 16/−14
Speleothems from cave walls covered by sediments from layers I-VII: youngest result is the maximum age of the archeo-palaeontological deposit in layers I-VII										
6	I-II	8033	Flowstone	2903	0.04	0.01	1.12 ± 0.09	8.668 ± 1.031		251.5 + 95.9/-51.7
7	II	8034	Stalactite	3003	0.23	0.05	1.11 ± 0.03	15.419 ± 1.106		261.8 + 42.0/−30.7
8	III	8035	Sparry calcite fragmet	1905	0.06	0.05	1.16 ± 0.07	3.944 ± 0.326		>300
9	IIIa	6914	Stalagmite	3314	0.25	0.07	1.15 ± 0.03	11.57 ± 1.34		194.4 + 20.2/−17.3
10	IIIa	6725	Stalagmite	3414	0.20	0.07	1.13 ± 0.03	14.36 ± 1.16		168.2 + 13.5/-12.1
11	IV	8036	Stalactite	2203	0.15	0.02	1.15 ± 0.03	20.004 ± 2.029		218.9 + 26.5/-21.6
12	V	8037	Stalactite	2804	0.14	****	1.21 ± 0.03	****		170.7 + 10.1/−9.4
13	VII	8038	Stalactite	2904	0.11	0.18	1.07 ± 0.03	1.885 ± 0.058		225.6 + 27.4/−22.0
14	VII	8039	Flowstone	3004	0.17	0.03	1.35 ± 0.04	17.798 ± 1.329		159.4 + 12.1/−11.0
Speleothems from cave walls covered by Layer VIII: maximum age for the beginning of sediment accumulation in the cave										
15	VIII	8040	Sparry Calcite	1805	0.07	0.09	1.01 ± 0.04	2.476 ± 0.108		>300
16	VIII	8041	Sparry Calcite	1205	0.03	0.01	1.24 ± 0.09	16.428 ± 2.857		>300
17	VII	8042	Sparry Calcite	1405	0.07	0.01	1.18 ± 0.04	38.233 ± 4.386		>300

[a] δ^{234} U measured = 310 ± 1‰, δ^{234} U initial = 406 ± 2‰.

polymineral fine grain samples from other Iberian karstic infill deposits (e.g., Berger et al., 2008). The lack of significant signal loss following laboratory storage may reflect: (i) the genuinely favourable athermal stability properties of the IRSL and TL signals measured for these samples; (ii) an absence, or near-absence, of feldspar grains in the silicate-rich, polymineral fine grain fractions measured here; or (iii) an artefact of the chosen laboratory measurements protocol.

Explanation (i) seems unlikely, as anomalous fading of feldspar IRSL and TL signals is a near ubiquitous problem that has been widely documented across a range of geological provinces (Aitken, 1985, 1998; Huntley and Lamothe, 2001). Explanation (ii) may be a contributory factor, as feldspars typically weather more rapidly than quartz in sedimentary environments (Nesbitt et al., 1996). Indeed, the feldspar contents of the sedimentary layers dated here are an order of magnitude smaller than the associated quartz

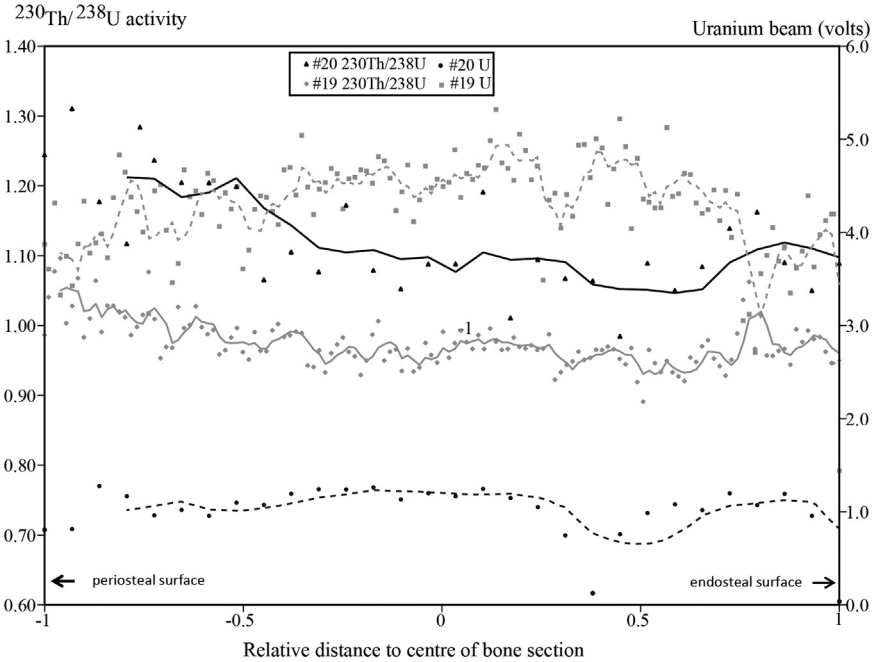

Fig. 3. $^{230}Th/^{238}U$ activity (solid line) and U 'concentration' (broken line) profiles across transverse sections of samples #19 and #20 measured by laser ablation MC-ICP-MS. The beam current at mass 238 is used as a proxy for uranium concentration. The lines represent a four-point moving average of the data.

Table 3
Dose rate data, multi-grain aliquot additive dose equivalent doses (D_e) and polymineral fine-grain IRSL and TL ages (1σ).

Sample ID	Site#	Layer	Method	Material	Lab#	Water content (%)[a]	*a*-value[b]	Total dose rate (Gy/ka)[c,d]	D_e (Gy)[d]	Age ka[d]
21	7409	I	TL	Sediment (2–10 μm)	MAD-4549	2	0.09	3.09 ± 0.09	269 ± 12	87.1 ± 4.8
22	7410	I	TL	Sediment (2–10 μm)	MAD-4558	2	0.16	3.10 ± 0.10	269 ± 13	86.8 ± 5.1
23	6848	II	IRSL	Sediment (2–10 μm)	MAD-5946BIN	6	0.17	3.31 ± 0.21	345 ± 14	104.1 ± 7.6
24	6821	IIIa	IRSL	Sediment (2–10 μm)	MAD-5925BIN	12	0.10	2.61 ± 0.05	335 ± 25	128.2 ± 9.1
25	6910	IIId	IRSL	Sediment (2–10 μm)	MAD-5926rBIN	7	0.07	2.19 ± 0.05	283 ± 20	129.4 ± 9.7
26	7404	Vsup	IRSL	Sediment (2–10 μm)	MAD-6071BIN	13	0.07	1.71 ± 0.10	246 ± 9	143.8 ± 9.8
27	7396	VIa/b	IRSL	Sediment (2–10 μm)	MAD-6070BIN	15	0.09	2.06 ± 0.05	318 ± 26	154.2 ± 12.0

[a] Field water content, expressed as % of dry mass of mineral fraction, with an assigned relative uncertainty of ±1%.
[b] Alpha effectiveness value used for alpha dose rate calculation, determined using the approach of Zimmerman (1971).
[c] Total dose rate comprises alpha, beta, gamma and cosmic-ray contributions. Beta and gamma dose rates were determined from ^{40}K, ^{238}U and ^{232}Th activities calculated on dried and homogenised, bulk sediment samples using a combination of beta counting and thick source alpha counting. The conversion factors of Nambi and Aitken (1986) were used to derive dose rate estimates from measured activities.
[d] Mean ± total uncertainty (1δ or 68% confidence interval), calculated as the quadratic sum of the random and systematic uncertainties.

contents (i.e., 0–7% versus 62–82%; Table 1). In spite of these relatively low feldspar contents, we cannot rule out the presence of a small number of feldspar grains in the aliquots used for D_e determination. Moreover, the inclusion of even a small number of feldspar grains may still be sufficient to dominate the measured TL and IRSL signals since feldspars display intrinsically brighter luminescence intensities than quartz grains. Explanation (iii) is noteworthy as there are a number of potential difficulties with deriving reliable fading assessments using non-normalised MAAD procedures (Aitken, 1998). More rigorous, sensitivity-corrected single-aliquot regenerative-dose anomalous fading tests were not performed on these samples following the widely adopted procedures of Huntley and Lamothe (2001) and Auclair et al. (2003).

In light of these considerations, it is possible that the TL and IRSL ages shown in Table 3 may slightly underestimate the true burial ages of these sediments as a result of unaccounted anomalous fading. However, the IRSL ages are in good agreement with the chronology obtained for layer II using ESR and AAR, and with the AAR ages for layers III and V. The IRSL ages obtained for layers III to VI are also consistent with the maximum ages established for these horizons using U-series dating of cave wall speleothems, while the TL ages for layer I are in close agreement with the U-series age established on the capping speleothem. The general concordance between the luminescence chronologies and the associated independent age estimates suggests that any systematic underestimation caused by anomalous fading may not be significant beyond the existing 2σ dating uncertainties. Alternatively, the effects of anomalous fading could have been masked by opposing systematic offsets such as partial bleaching (Arnold et al., 2007, 2011; Arnold and Roberts, 2011), which can be difficult to ascertain in multiple-aliquot/multiple-grain studies (Arnold and Roberts, 2009; Arnold et al., 2012).

In sum, the luminescence results are in broad agreement with U–Th ages and suggest that Unit 1 (layers I-III) was likely deposited in MIS 5. The luminescence result for Unit 2 (layers V) and the upper part of Unit 3 (layers VI) are consistent with the maximum age of ~160 ka obtained by U–Th for layer VII.

4.2.3. Amino acid racemisation

The GC data for these samples can be directly compared with the aspartic acid, glutamic acid and phenylalanine D/L values calculated by HPLC on the grounds of similarities found between the racemisation ratios of samples from Wehmiller's (1984) inter-laboratory comparison (ILC) study, as well as several GC and HPLC comparisons performed on samples in our laboratory (Ortiz et al., 2009).

Similarly, for isoleucine, the values obtained by HPLC and GC did not require transformation as the D-alle/L-Ile ratios measured by HPLC were below 0.45 (cf. Wehmiller, 1984; Torres et al., 1997; Ortiz et al., 2004; Wehmiller et al., 2010).

The mean D/L values for aspartic acid, glutamic acid, phenylalanine and isoleucine of *Testacella haliotidea* opercula are shown in Table 4 for each sample, together with the numerical ages for samples #28 to #42. The final age of each sample has been calculated as the average of the various age estimates obtained for each amino acid D/L value. The associated age uncertainties quoted in this study represent the standard deviation of the various age estimates obtained from the D/L values of each sample.

The amino acid racemisation ages were calculated using the algorithms established by Torres et al. (1997) for the central Iberian Peninsula. The use of these algorithms for dating the Cova del Rinoceront deposits is justified because a similar thermal history can be inferred for the central and eastern regions of the Iberian Peninsula, i.e., the site lies within the same Mediterranean-pluviseasonal climatic zone and has a similar Current Mean Annual Temperature (CMAT) (Rivas-Martínez and Rivas-Sáenz, 1996–2009).

Within their large uncertainties, the AAR results are consistent with the U–Th and luminescence ages for Units 1 and 2 and further suggest that the endokarstic fill making up Unit 3 was not deposited much earlier than the time of opening of the cave to the surface.

4.2.4. ESR

Peak heights were analysed for the g = 2.0007 signal and used to derive an AD (accumulated, or total, dose) of 463.7 ± 20.1 Gy for the tooth specimen. To convert the AD to an age, estimates were made of external and internal dose rates. Neutron Activation Analysis (NAA) of dentine and sediment were used to determine concentrations of major radioisotopes. Cosmic radiation was assumed to be negligible, and the sediment water content was assumed to average 15% (sample #43a).

ESR dating of teeth is complicated by the uptake of uranium from ground water into the dentine, and to some extent into the enamel. Several uptake models have been suggested to reconstruct complex post-burial uranium histories. The early uptake (EU) model assumes that all the uranium was absorbed shortly after burial. The linear uptake (LU) model assumes that uranium has been taken up continuously during burial. The recent uptake (RU) model, which is rarely used, assumes that some event occurring shortly before excavation caused increased uranium uptake. More complicated uptake patterns are also possible but can be difficult to model effectively. To determine the post-burial uranium uptake history with greater precision, it is possible to couple ESR and U-series dating, as long as the sample is large enough and contains

Table 4
Aminoacid racemisation ages (2 σ).

Sample ID	Site#	Layer	Material	Lab#	Weight (mg)	D/L Asp	D/L Glu	D/L Phe	D-allo/L-Ile	Age ka
28	8011	II	*Testacella haliotidea*	12996	1.8	0.580	0.262	0.405	0.276	99 ± 22
29	8010	III	*Testacella haliotidea*	13013 to 13016	12.2 to 18.5	0.621 ± 0.007	0.280 ± 0.008	0.518 ± 0.022	0.290 ± 0.007	126 ± 34
30	7883	III	*Testacella haliotidea*	13021 to 13024	12.2 to 15.2	0.629 ± 0.019	0.296 ± 0.019	0.560 ± 0.038	0.303 ± 0.031	140 ± 46
31	7884	III	*Testacella haliotidea*	13017 to 13020	13.4 to 17.8	0.630 ± 0.018	0.294 ± 0.014	0.562 ± 0.041	0.316 ± 0.026	142 ± 46
32	7885	III	*Testacella haliotidea*	13009 to 13012	8.8 to 17.7	0.627 ± 0.004	0.285 ± 0.004	0.521 ± 0.013	0.289 ± 0.013	128 ± 35
33	7405	V	*Testacella haliotidea*	13001 to 13004	8.2 to 11.3	0.637 ± 0.005	0.300 ± 0.003	0.547 ± 0.023	0.332 ± 0.016	144 ± 38
34	7407	V	*Testacella haliotidea*	12997 to 13000	7.7 to 14.5	0.699 ± 0.005	0.350 ± 0.004	0.677 ± 0.026	0.411 ± 0.011	209 ± 79
35	8015	V	*Testacella haliotidea*	4746	79.8	0.660	0.279	0.487	0.423	165 ± 23
36	8016	VI	*Testacella haliotidea*	4745	77.1	0.727	0.331	0.583	0.539	230 ± 27
37	8017	VI	*Testacella haliotidea*	4741	76.6	0.691	0.316	0.579	0.458	205 ± 20
38	7397	VI	*Testacella haliotidea*	13029 to 13031	8.1 to 9.2	0.704 ± 0.005	0.368 ± 0.007	0.710 ± 0.004	0.437 ± 0.002	228 ± 92
39	8018	VII	*Testacella haliotidea*	4740	80.4	0.691	0.301	0.559	0.463	200 ± 19
40	8019	VII	*Testacella haliotidea*	4743	80.6	0.715	0.326	0.574	0.541	227 ± 22
41	8020	VII	*Testacella haliotidea*	4744	74.6	0.726	0.330	0.583	0.539	230 ± 26
42	7403	VII	*Testacella haliotidea*	13005 to 13008	7.0 to 14.9	0.686 ± 0.007	0.352 ± 0.008	0.625 ± 0.017	0.499 ± 0.025	190 ± 52

sufficient U. This was not done for sample #43, both because of limited sample size and because of the higher analytical costs. As a result, Table 5 shows the ages obtained for sample #43 using the EU and LU models. There is no reason to consider an RU model in the present context.

Sample #43 was collected in layer II, and its EU enamel age is in good agreement with the IRSL age obtained for the same layer (sample #23) and the U–Th age on Proboscidean tusk for layer III (sample #18), while the LU age is considerably older. It is worth noting that the quoted ESR errors do not take into consideration several systematic factors. In particular, the external dose rate is based purely on a single, laboratory-analysed sediment sample rather than on in situ measurements. As this sedimentary layer is 'lumpy', it is possible that the true dose rate might have been influenced by fallen rocks and other sedimentary elements that were not captured by the laboratory sample. Recalculating the external dose rate with different assumptions suggests that this is not the most likely source of uncertainty. The internal dose from dentine and enamel is by far the greater contributor to the total dose rate, which helps diminish the effects of external dose rate variations. The dentine dose rate is more than double that of the enamel. Comparing the relative amounts of U in the dentine and enamel, it seems likely that the EU model may well provide the best age estimate for this specimen; though the possibility remains that an intermediate age between the EU and LU model is also suitable. Further samples would need to be tested to resolve this issue – preferably samples that are large enough to permit coupled ESR/U-series dating.

4.2.5. Palaeomagnetic data

Palaeomagnetic directions were determined for each sample using least-square fit of at least six successive temperature steps within the 350°C–600 °C temperature range (Fig. 4). Samples #45, #46 and #47, all from Unit 3, yielded north-westerly declinations with positive (down) inclinations. Given the location of the study site in the mid-latitudes of the northern hemisphere, these directions are indicative of a normal polarity geomagnetic field. In contrast, sample #44, from the base of Unit 2, yielded a southerly declination with negative (upwards) inclination, this is indicative of a reversed polarity geomagnetic field.

The occurrence of normal polarity magnetisations in three out of four samples is coherent with an age younger than the 0.78 Ma age of the Brunhes/Matuyama boundary. The interpretation of a single sample with reversed polarity is not easy, as we cannot rule out the possibility that it corresponds to a reworked mud fragment. Whether this sample records a short reversed geomagnetic event within the Brunhes epoch is uncertain (Chanell et al., 2006). Among the latter, the Iceland Basin geomagnetic event has been documented in different locations around the globe at ~188 ka. Other intra-Brunhes excursion events, such as Calabrian Ridge and Fram Strait (155–165 ka) could also explain the polarity reversal for the late Middle Pleistocene horizon at this site.

4.3. Stone tools

The lithic assemblage from Cova del Rinoceront consists of very few artefacts: 22 in total. Ten artefacts were found in the fallen sediments accumulated at the foot of the section and their stratigraphic origin is therefore unknown. These artefacts were described in a previous paper (Daura et al., 2005). Five of the objects are made of quartz, three of flint and two of limestone; all of these raw materials are available in the vicinity of the deposit. All the quartz remains are flakes and flake fragments. Two of the flint items are cores and the third is a retouched artefact. The most significant find is a core on small pebble that shows a structure characterised by two opposing surfaces: a flat flaking surface presenting centripetal removals and a convex surface used to prepare the striking platforms (Fig. 5-1). This hierarchical structure is similar to that characterising the Levallois technique, although it may be partly explained by the reduced size of the cobble. The second core is very small (22 × 19 × 17 mm) and shows a polyhedral appearance (Fig. 5-4). It corresponds to a reduction sequence aimed at the production of blanks smaller than 2 cm. The third flint item is a small retouched artefact that exhibits a notch on the left side and an inverse removal at the proximal end; this removal

Table 5
Radioisotope content, annual dose rates and ESR ages (1 σ).

Sample ID	Site#	Layer	Lab#	Material	U (ppm)	Th (ppm)	K (%)	Water content	Dose rate (mGy/a)	AD (Gy)	EU age ka	LU age ka
43a	6848	II	PT76 sed	Sediment	3.28	9.95	1.02	15%	0.948 ± 0.064			
43b	5733	II	PT76 den	*H. mediterraneus* DP4 dentine	37.58	1.26	0.08					
43c	5733	II	PT76 en	*H. mediterraneus* DP4 enamel	7.42					464 ± 20	93 ± 7	160 ± 11

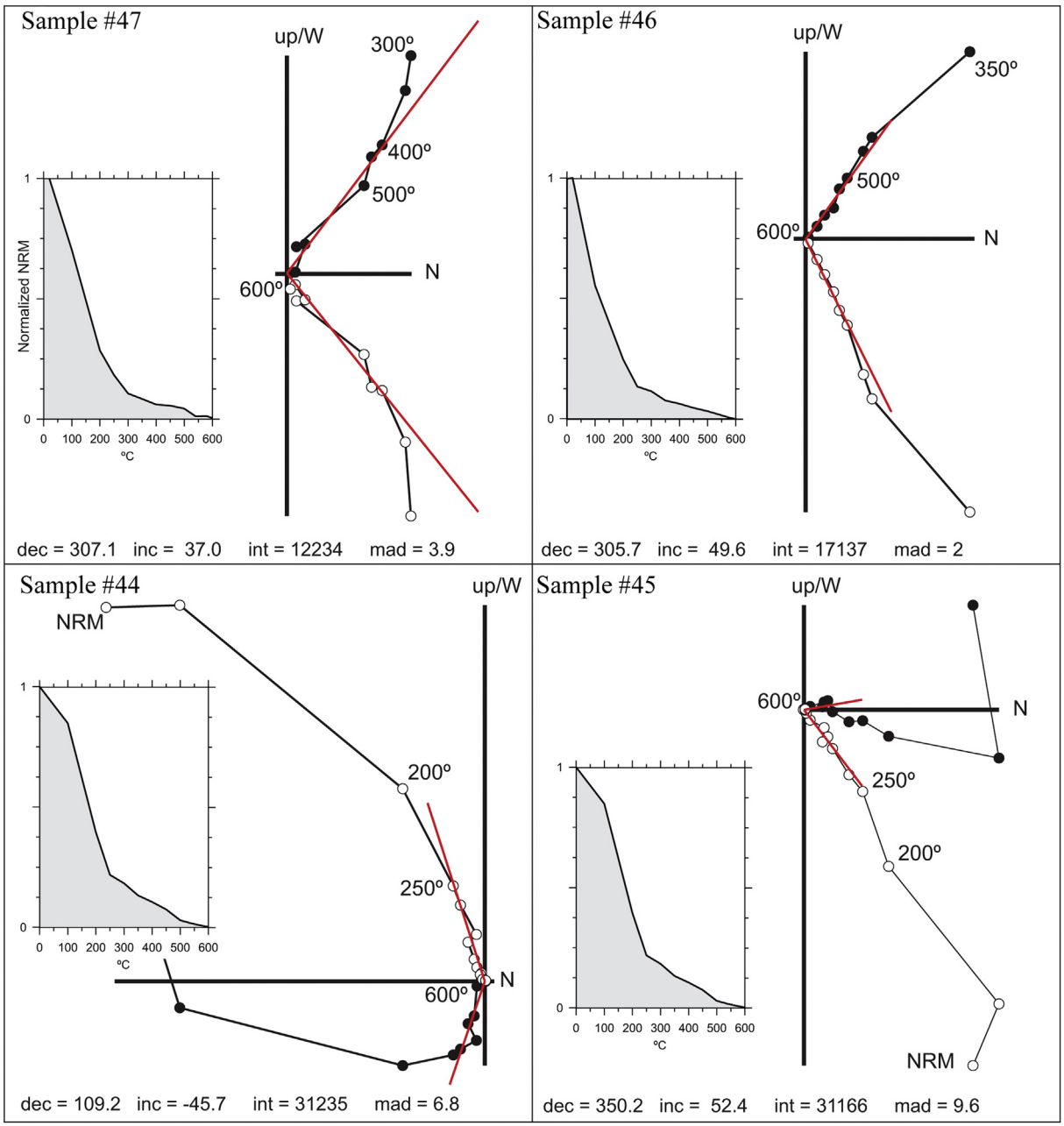

Fig. 4. Vector endpoint diagrams of stepwise demagnetisation data from all studied samples and associated NRM decay plots during thermal treatment. Red lines represent calculated palaeomagnetic directions (int: intensity in 10^{-6} A/m; mad: maximum angular deviation). (For interpretation of the references to colour in this figure legend, the reader is referred to the web version of this article).

created a striking platform that was used to strike a series of small detachments on the dorsal face of the blank (Fig. 5-12). Finally, the limestone artefacts include a flake fragment (Fig. 5-15) and an unworked cobble (Fig. 5-6).

The assemblage recovered during the excavation of layers I to III consists of mostly small-sized artefacts: six from layer I, five from layer II and one from layer III. In this case, flint is the dominant raw material (nine artefacts), followed by quartz (three artefacts). All the flint artefacts exhibit an intense white patina and most of them show evidence of mechanical damage on the edges, suggesting that the assemblage was subjected to significant post-depositional weathering. In addition, one flint found in the excavation – as well as the retouched artefact found out of stratigraphical context – show evidence of fire damage. Nine remains have a maximum length smaller than 25 mm. All the quartz remains and six flint items are flake and flake fragments. There are also three retouched artefacts on flint. The first was found in layer I and it is a small flake (20 × 25 × 9 mm) showing a notch on its distal edge (Fig. 5-7). The second was recovered from layer II and it is also small artefact (23 × 15 × 6 mm), presenting a marginal retouch on the distal edge (Fig. 5-17). Finally, the third retouched implement is a flake that exhibits an abrupt retouch on the right side (Fig. 5-16).

This small assemblage yields little information about the psycho-technical strategies or the techno-economical organisation, but it is clear evidence for human presence around the cave. In the

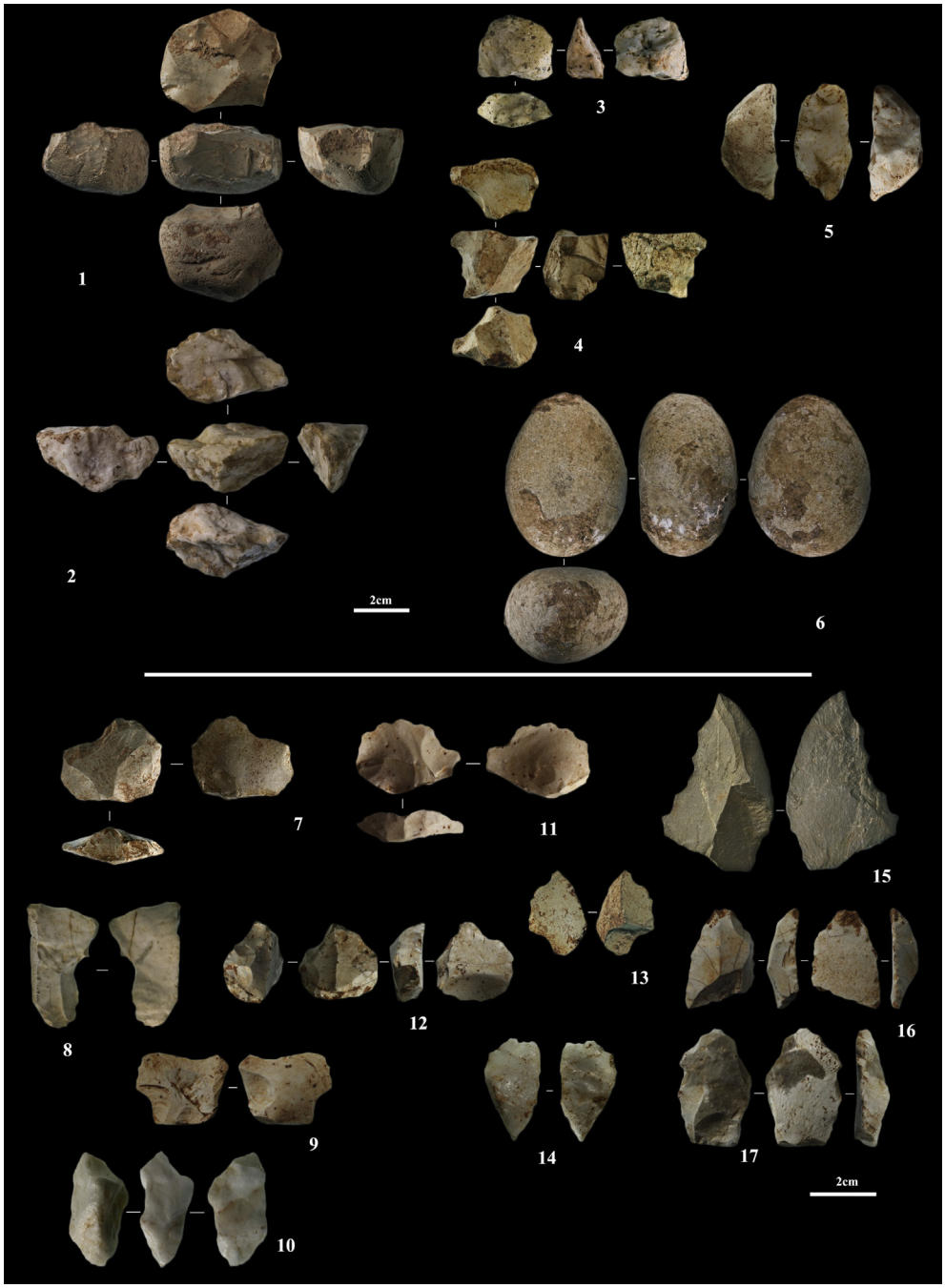

Fig. 5. Lithic artefacts from Cova del Rinoceront. 1: Flint core showing a preferential flaking surface with centripetal removals. 2: Quartz flake fragment. 3: Quartz flake. 4: Small polyhedral core on flint. 5: Quartz flake fragment. 6: Limestone cobble. 7: Retouched flint artefact with a notch on the distal edge. 8: Flint flake. 9: Flint flake. 10: Quartz flake fragment. 11: Flint flake. 12: Retouched flint artefact showing a distal notch and a convex retouch in the proximal end. 13: Flint flake. 14: Quartz flake fragment. 15: Limestone flake fragment. 16: Retouched flint artefact with abrupt retouch of the right side. 17: Retouched flint artefact presenting a marginal retouch in the distal edge. 1, 3–6, 12 and 15 were found out of stratigraphic context. 2, 7–11, 13–14 and 16–17 were recovered during the excavation of layers I to III.

excavated area no on-site stone tool knapping has been documented. The artefacts therefore document human activity elsewhere in the cave or outside, the latter strongly intimated by the evidence of post-depositional damage, indicative of a non-primary position. In this context, the small size of the recovered items, including cores, could be explained by size sorting processes (gravity or wash) associated with post-depositional transport. These lithic artefacts indicate human presence in the surrounding areas forming the sedimentary catchment of the site.

4.4. Bioarchaeological record

The palaeoenvironmental sampling program undertaken at Cova del Rinoceront has revealed the presence of a wide range of bioarchaeological remains, namely phytoliths, charcoal, large vertebrates and small vertebrates. The samples have been obtained from collapsed sediments, the excavated layers (I, II and III) and the test pit into the bottom of the sequence (layers VI, VII and VIII). A more detailed study of this environmental evidence is ongoing. The

Table 6
Faunal species represented in Cova del Rinoceront.

	Layer I		Layer II		Layer III		Layer IV		Layer V		Layer VI		Layer VII		Layer VII–VIII		Layer VIII		Rubble	
	NISP	NMI	NISP	NMI	NISP	NMI	NISP	NMI	NISP	NMI	NISP	NMI	NISP	NMI	NISP	NMI	NISP	NMI	NISP	NMI
Carnivora																				
Canis lupus			4	1																
Crocuta sp.																			18	1
Felis cf. *silvestris*																			1	1
Lynx pardinus	91	4																		
Ursus arctos	1	1																	1	1
Perissodactyla																				
Stephanorhinus hundsheimensis					2	–													60	4
Artiodactyla																				
Bos/Bison	7	1																	5	1
Capra sp. & *Capra* cf. *ibex*	66	5	1	2															12	2
Capreolus sp.																			22	2
Cervus elaphus	41	1																	4	2
Haploidoceros mediterraneus	623	12	59	6	34	1														
cf. *Hemitragus* sp.																			1	1
cf. *Cervidae/Capridae*	74		32																	
cf. *Cervidae*	42																		4	
Proboscidea																				
Proboscidea indet.					54	1													1	1
Lagomorpha																				
Leporidae	766	21	12	2																
Testudines																				
Testudo hermanni	58	2	23	2	265	23													~1250	11
Caudata																				
Salamandra salamandra					1	1														
Anura																				
Pelobates cultripes	4	1	12	2	14	3							1	1			3	2		
Bufo bufo					41	4			44	4	1	1	16	4			14	3		
Pelophylax sp.													3	3			5	2		
Anura indet.									1				1				1			
Squamata																				
Timon lepidus					1	1														
Anguis fragilis					2	1			2	2			53	4						
Natrix natrix	38	1	2	1	3	1							1	1	1	1	6	1		
Coronella girondica									1	1										
cf. *Coluber* sp.					16	1														
Malpolon monspessulanus													49	5	2	1	31	3		
Rhinechis scalaris	4	1	4	1																
Colubrinae#1													2	1						
Colubrinae indet.	3			1									21				7			
Vipera sp.	1	1											3	2			3	2		
Ophidia indet.	4			3	5								47				33			
Erinaceomorpha																				
Erinaceus europaeus	2	1	4	2					1	1										
Soricoforma																				
Talpa cf. *T. europaea*	1	5	13	6	22	11							7	3	1	1	4	2		
Sorex sp.													1	1			1	1		
Crocidura cf. *C. russula*	5	3	2	1									11	5	1	1	2	1		
Chiroptera																				
Rhinolophus ferrumequinum													1	1						
Rhinolophus gr. *euryale-mehelyi*	1	1																		
Rodentina																				
Iberomys brecciensis	18	9	24	12	24	12							14	7	1	1	8	4		
Microtus (*Terricola*) sp.													1	1						
Myodes glareolus	1	1									1	1	4	2						
Apodemus cf. *A. sylvaticus*	19	9	12	6	5	3			1	1	2	1	128	64	11	5	6	3		
Eliomys quercinus	7	4	7	4	1	1							3	2						
Glis cf. *G. glis*					12	6			2	1	1	1	3	15						
Galliformes																				
Alectoris cf. *rufa*	2	2	1	1	1	1														
Columbiformes																				
Columba livia/C. oenas	2	1	2	1																
Piciformes																				
Picus viridis	1	1																		
Passeriformes																				
Galerida sp.	1	1																		
Calandrella brachydactyla	1	1																		
Parus major	1	1																		
Turdus sp.	5	3	1	1																
Luscinia cf. *megarhynchos*			1	1																
Fringilla coelebs	1	1	1	1																
Pyrrhula pyrrhula	3	3																		
Loxia curvirostra	1	1																		

Table 6 (*continued*)

	Layer I		Layer II		Layer III		Layer IV		Layer V		Layer VI		Layer VII		Layer VII–VIII		Layer VIII		Rubble	
	NISP	NMI	NISP	NMI	NISP	NMI	NISP	NMI	NISP	NMI	NISP	NMI	NISP	NMI	NISP	NMI	NISP	NMI	NISP	NMI
Plectrophenax nivalis	1	1																		
Corvus antecorax	3	1																		

results discussed below focus on the presence and absence of particular species, rather than rigorous statistical analyses (since palaeontological restoration is still in progress). However, a number of interesting observations can be made from these data.

4.4.1. Macrofauna

Large vertebrate remains have been recovered throughout the stratigraphic sequence. Most of the materials discussed herein came from layer I, where 87% of the sample has been already restored. The materials from layers II and III are covered by a breccia matrix and are still under preparation, but a preliminary assessment is provided (Table 6).

Layers I and II have a similar faunal composition and few coprolites (NR = ~65) have been recovered (Fig. 6-5). Layer I yielded a rich and well-preserved large vertebrate assemblage with ~1800 remains. Layer II contains ~680 remains. In these two layers, the medium-sized deer *Haploidoceros mediterraneus* is the predominant ungulate species in terms of the number of individuals (MNI = 12 for layer I) (Figs. 6-2 and 6-4) followed by *Capra* cf. *ibex* (MNI = 5 in layer I). The presence of the latter is based on the horn bases of an adult individual skull, which are narrow and straight in frontal view and lean backward in lateral view. Horn cores diverge at an angle of 40° in frontal view, have a sub-triangular basal section (flattened in anterior view and rounded in posterior view) and are compressed in transversal section. Both the horn cores and the preserved upper M3 are consistent with features of the ibex (Cregut-Bonnoure, 2005), and therefore we preliminary assign this material to *Capra* cf. *ibex* (Fig. 6-1).

The red deer, *C. elaphus*, is represented in layer I by a partial skeleton (MNI = 1); it corresponds to a senile female based on the absence of antler pedicles in the recovered skull. A large infantile bovid (*Bos*/*Bison*, MNI = 1), represented by deciduous teeth, is also found in layer I but the genus cannot be determined (Fig. 6-3).

In layer I, the only carnivores are lynx (*Lynx pardinus*, MNI = 4) (Fig. 6-6) and brown bear (*Ursus arctos*, MNI = 1). The latter is represented by a shed deciduous tooth (upper dp4), indicating the presence at the site of an individual aged from around the time of first milk dentition replacement (around 5–6 months postnatal) (Sanz, 2013).

Preliminary analysis indicates that the ungulate remains from layer II are of similar taxonomic composition. Among the carnivores, however, no bear remains have been identified; instead, there is a single individual of wolf (*Canis lupus*) (Fig. 6-7).

The most relevant feature of these layers is the presence of *Haploidoceros mediterraneus*, a deer that until now had only been documented at two late Middle Pleistocene sites in the south of France, Lunel-Viel (Hérault) and Igue des Rameaux (Tarn-et-Garonne) (Croitor et al., 2008). The anatomical characteristics of the cervid remains allow us to rule out *Dama*, even though this taxon is often cited at other MIS 5 Iberian Peninsula sites, such as Cueva del Camino (Álvarez-Lao et al., 2013), Bolomor, or Cova Negra (Martínez del Valle, 1996, 2001). The recovery of several, almost complete crania, together with two sickle-shaped beams and a long frontal basal tine with the anatomical features described by Sanz et al. (2014) establishes for the first time the presence of *Haploidoceros mediterraneus* in the Iberian Peninsula, extending its chronological range to MIS 5. The absence of the species at younger sites from the adjacent geography, including the MIS 3 sites of Cova del Gegant and Cova del Coll Verdaguer, as well as from the Heinrich Stadial 4 horizon of Terrasses de la Riera dels Canyars (Daura et al., 2013), suggests that its regional extinction occurred at the beginning of the Last Glacial period.

Layer III has only been partially excavated, but several different horizons of fossil assemblages can be identified. The upper part (sub-layer IIIa) is characterised by several remains of an immature cervid, probably *Haploidoceros* (~50 remains). The most relevant feature of sub-layers IIIa and IIIb is the dominance of *Testudo hermanni* remains (Fig. 7-7), especially in IIIb, where ungulates (including *Haploidoceros*) and carnivores are absent. In layer III, *Testudo* remains are significantly more abundant (NISP = 265 and MNI = 23) than in layers I (NISP = 58) and II (NISP = 23). Tortoise remains in most cases preserve the complete shell or partially complete shells (Fig. 7-7). Skeletal elements are also abundant and sometimes the proximal limbs were found in anatomical position. There are also many isolated scutes in this layer. It is plausible that a great part of the tortoise remains (MNI = 11) recovered from the rubble (Daura et al., 2006) come from this layer; if so, the tortoise MNI would be considerably higher for layer III.

An articulated elephantid skeleton has been found in sub-layer IIIc (Fig. 1-6), although it has not yet been removed from the site. These remains correspond to a complete, immature specimen but the current condition does not permit taxonomic determination as *Mammuthus* or *Elephas*. An additional proboscidean pisiform bone found in the rubble deposits indicates the presence of a second individual. Both genera were present in Europe during the time range of layer III, so either could be present at this site. *Elephas antiquus* became extinct in Europe at the end of MIS 5e, although a late survival is suggested for southern regions (Stuart, 2005; Mol et al., 2007).

Several rhinoceros remains have been observed and recovered (IIIe) from the stratigraphic profile underlying the elephantid skeleton (Figs. 7-1 to 7-6). This layer IIIe is still not excavated, but similar specimens have been collected from the rubble, and may originate from this same layer. The total rhinoceros NISP for sublayer IIIe and rubble is 62, for a MNI of 4 (3 adults and 1 juvenile). Among these remains, two belong to a skull coming from sublayer IIIe: an anterior fragment of the nasal bone, and a posterior skull area with the orbitotemporal fossa, the ear region and the occipital face. Two mandibular fragments have been also recovered, one with P4 and M3 and another corresponding to the ascending ramus; the remaining finds are isolated upper and lower teeth, and postcranial elements. The nasal fragment is only slightly rugose and not very bulging. This specimen therefore resembles the skull of *Stephanorhinus etruscus* from Capitone (Ambrossetti, 1972), but is different from that found at Chilhac (Boeuf, 1995), which is more convex and rugose. The development of a nasal bump is weaker than in *Stephanorhinus hundsheimensis* (Fortelius et al., 1993).

The cranial fragment (Fig. 7-6) is relatively small, with an acute occipital vertex that is not very expanded. The occipital face is high and barely inclined backward, which coincides with the features of *S. etruscus* (Guérin, 1980, referred to as *D. e. etruscus*). The low elevation of the occipital with respect to the preserved frontal area is consistent with *S. hundsheimensis* (Fortelius et al., 1993; Mazza et al., 1993; Sala and Fortelius, 1993). The external auditory

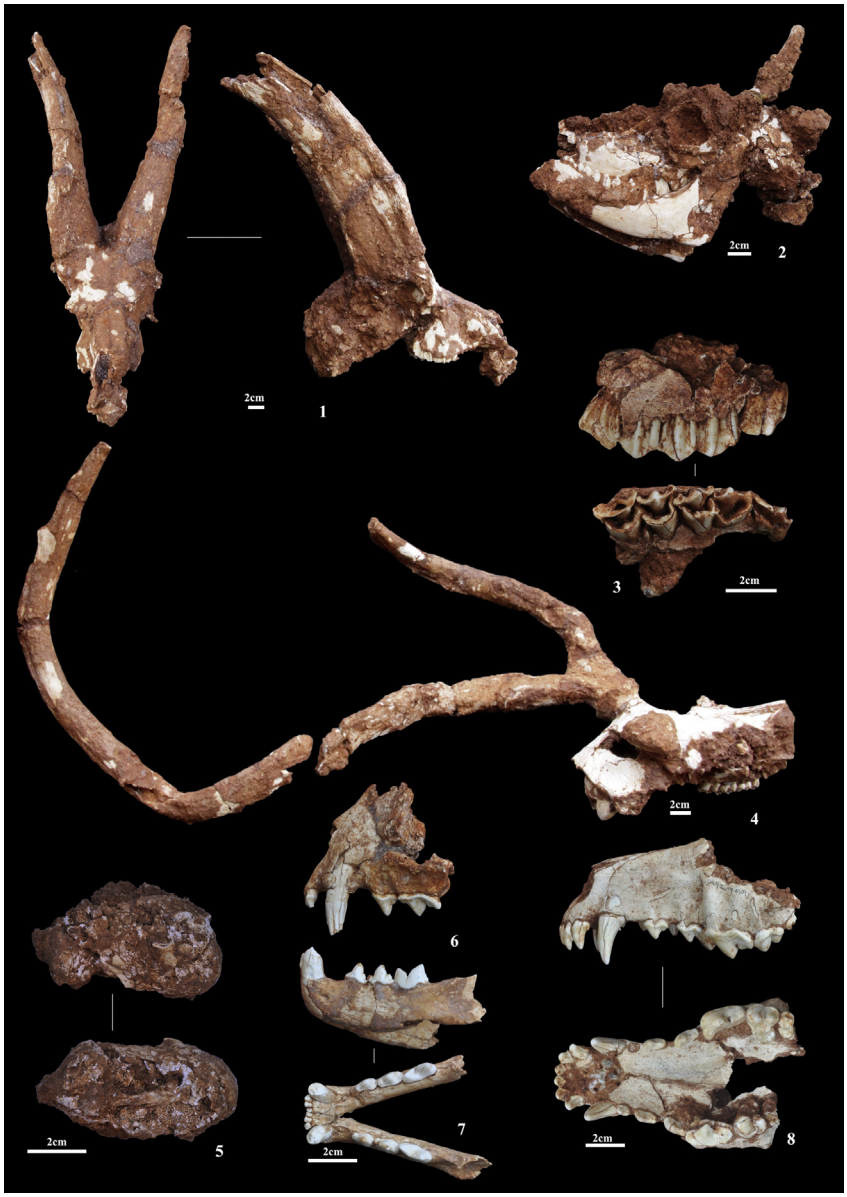

Fig. 6. Faunal remains of layer I. 1: *Capra* cf. *ibex* cranium. 2: *Haploidoceros mediterraneus* juvenile skull. 3: Infantile large bovid maxilla. 4: *Haploidoceros mediterraneus* adult cranium. 5: Carnivore coprolite. 6: *Lynx pardinus* maxilla and mandible. 7: *Canis lupus* maxilla.

meatus is ventrally closed as observed in both *S. etruscus* and *S. hundsheimensis*. Concerning size, the occipital height reaches the maximum value reported so far for *S. etruscus* (Guérin, 1980; Mazza, 1988), whereas the remaining dimensions fall within typical ranges and are closer to the minimum reported values.

The ascending mandibular ramus exhibits a slight forward inclination, as is common for *S. etruscus* (Guérin, 1980). The mandibular dimensions are also close to the minimum values obtained for *S. etruscus* (Guérin, 1980; Fortelius et al., 1993).

The upper dentition is characterised by the presence of cementum, filling the valleys in some cheek teeth as in M3 (Fig. 7-2). Dental morphology and size are rather similar between *S. etruscus* and *S. hundsheimensis*, and some features differ only in their statistical representation; for instance, the absence of cingulum in P4 (Fig. 7-3) is statistically more common in *S. hundsheimensis* (Fortelius et al., 1993).

The postcranial skeleton is represented by several fragments of ulna, femur, tibia, metacarpals, carpus, tarsus and phalanges. Even though no complete bone is preserved, the metapodial fragments are slender, with clear concave articulations, which point to good running capabilities. As with the tooth remains, the postcranial morphology is also consistent with both *S. etruscus* and *S. hundsheimensis*. In particular, the trapezoid, the proximal facet of Mc III, the femur and the ectocuneiform are close to those of *S. hundsheimensis* from Isernia, Moschbach and Mauer (Fortelius et al., 1993), although their dimensions tend toward the minimum values of *S. etruscus* (Guérin, 1980). In turn, the cuboid and the articular facet of Mt IV are similar to the homologous bones of *S. etruscus* from Poggio al Pero (Valdarno) (Fortelius et al., 1993), and their dimensions fit well within the variability range of *S. etruscus* (Guérin, 1980; Fortelius et al., 1993). Morphologically, these rhinocerotid remains are closer to the Lower-Middle Pleistocene species (i.e., *S. etruscus* and *S. hundsheimensis*) than to the late Middle-Upper Pleistocene ones (*S. hemitoechus* and *S. kirchbergensis*). Based on skull and mandibular features, as well as in size, we assign these remains

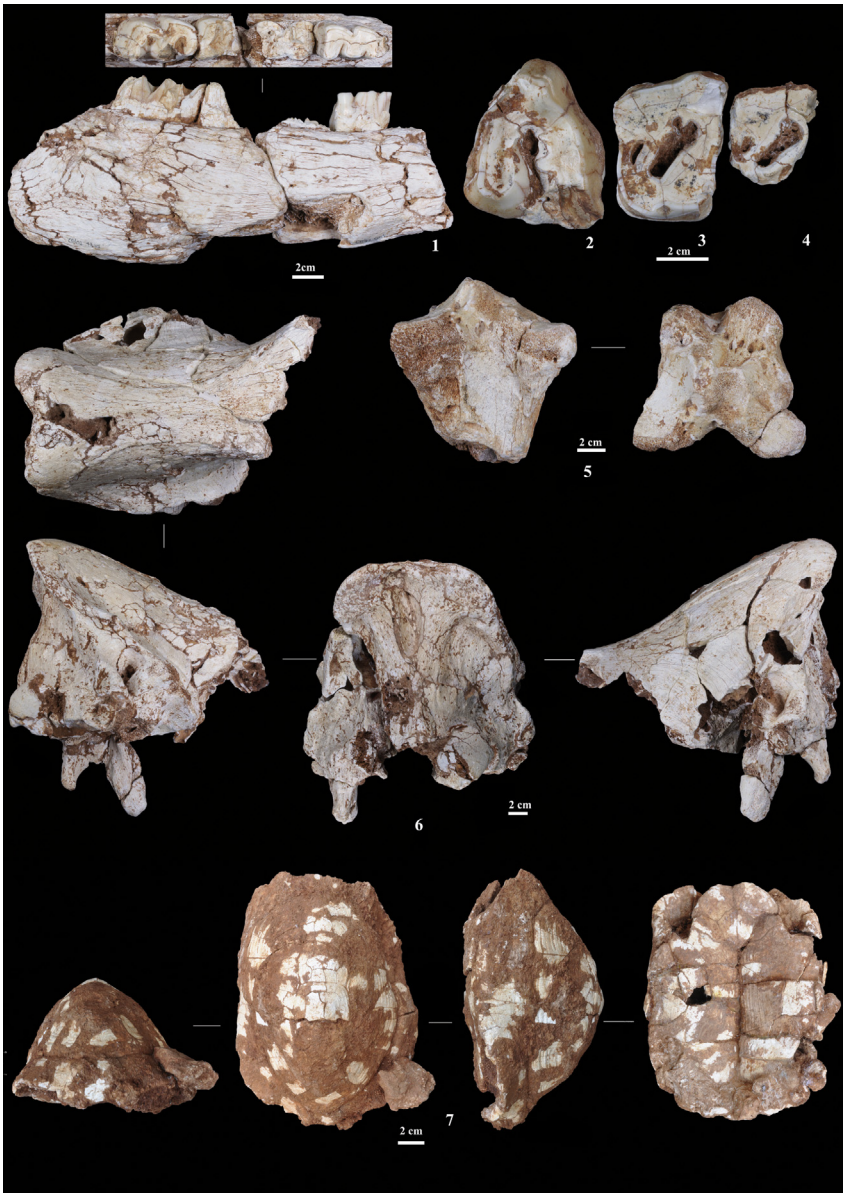

Fig. 7. Faunal remains of layer III. 1: *Stephanorhinus hundsheimensis* left hemi-mandible with P4 and M3. 2: *S. hundsheimensis* upper left M3. 3: *S. hundsheimensis* upper right P4. 4: *S. hundsheimensis* upper right P3. 5: *S. hundsheimensis* left tibia. 6: *S. hundsheimensis* posterior cranium fragment. 7: *Testudo hermanni* carapace (7).

to *S. hundsheimensis*, even though, elsewhere, this taxon remains unrecorded after ~500 ka.

The most significant finding from the test pit into layers VI, VII and VIII is an articulated partial axial skeleton of a large mammal that might be related with some of the large bovid (*Bos*/*Bison*) remains recovered from the rubble. Other vertebrate remains from these layers include roe deer (*Capreolus* sp.) and the Mediterranean tortoise (*T. hermanni*) (Daura, 2008).

In addition to the taxa found in situ within the stratigraphic profile, the rubble sediments have also provided remains of species such as the carnivores *Crocuta* (NISP = 18) and *Felis* cf. *silvestris* (NISP = 1) and the bovid cf. *Hemitragus* (NISP = 1). Other remains recovered from the rubble are too fragmented to yield identifiable taxonomical or anatomically features; indeed, out of the large number of recovered remains (NR = 17,933), the vast majority are splinters (NR = 17,615).

4.4.2. Microfauna

The water-screened and hand-picked sediments of the Cova del Rinoceront sequence have yielded 968 identifiable small vertebrate remains. These remains comprise at least 25 taxa (Table 6). The most abundant material comes from the systematically excavated upper part of the sequence (layers I to III) and from layer VII of the test pit.

From a biochronological perspective, the presence of the rodent species *Iberomys brecciensis* is significant (Ayarzagüena and López Martínez, 1976; López-García, 2008; López-García et al., 2008, 2011; Maroto et al., 2012). *I. brecciensis* is an extinct vole, which disappeared around the Middle-Upper Pleistocene transition. This vole is the ancestor of the extant *Iberomys cabrerae*, which is first found in the Iberian Peninsula at the ~74.5 ka Cueva del Camino site (Arsuaga et al., 2010; Laplana et al., 2013). On the basis of this evidence, therefore, the Cova del Rinoceront sequence should predate the MIS 4-MIS 5a transition.

The presence of *Glis glis* (fat dormouse) in layers III and VII is also of interest. *G. glis* is a rodent that appeared in southern Europe during the late Middle Pleistocene, during MIS 13 or MIS 12 (ca 420 to 530 ka), at sites such as l'Arago (France) (Desclaux, 1992; Hanquet, 2011) and Fontana Marella (Italy) (Bona et al., 2008). This species is also found in France during MIS 6 at Lazaret and Moula-Guercy (Hanquet, 2011), and is associated with MIS 5e deposits at Borisova (Russia) (Markova, 2000) and Burgtonna (Germany) (Kolfschoten, 2000).

The abundance of the rodents *Iberomys brecciensis* and *Apodemus* cf. *A. sylvaticus* throughout the sequence indicates a landscape dominated by open forest and mild climatic conditions. Warm conditions are also indicated by the presence of the snakes *Rhinechis scalaris* (layers I-II) and *Malpolon monspessulanus* (layers VII.-VIII). The presence of the mole *Talpa* cf. *europaea* throughout the sequence, as well as *Salamandra salamandra*, *Anguis fragilis*, *Natrix natrix* and to a lesser extent *Bufo bufo*, indicates slightly more humid conditions than today. The occurrence of the toad *Pelobates cultripes* implies loose and sandy soils in the area, while the frog *Pelophylax* sp. indicates the presence of water in the vicinity of the cave.

Taken together, the microfaunal evidence indicates that the upper part of the sequence (layers I to III) relates to MIS 5, in agreement with chronometric dating results. The abundance of the rodent species *I. brecciensis* and *G. glis*, together with the rest of the small-vertebrate association, consistent with a Mediterranean climate, suggest that layer III probably corresponds to MIS 5e. Given that the maximum age indicated for layer VII by U–Th (~175 ka) implies that layer VII post-dates MIS 7, the lower part of the sequence, in particular layer VII, could relate to a warm phase during MIS 6. The layer VII assemblage is very similar to other small vertebrate associations from the Mediterranean zone, such as Bolomor layer 5 (dated to ca 228 ka; Guillem-Calatayud, 2000), Mollet cave (dated to ca 215 ka; Maroto et al., 2012; López-García et al., 2014), the Upper sequence (TE18-19) of Sima del Elefante (MIS 7 to MIS 9; Blain et al., 2011; López-García et al., 2011), Valdocarros (MIS 7 to MIS 8; Sesé et al., 2011; Blain et al., 2012), la Baume Bonne (MIS 7 to MIS 8; Hanquet, 2011) and Cèdres (MIS 7; Hanquet, 2011).

4.4.3. Birds

A total of 13 avian taxa (genera and species) have been found in Cova del Rinoceront (Table 6). Layer I is the richest, with 11 taxa; in layer II, six taxa are represented; remains from one species only, *Alectoris* cf. *rufa*, were unearthed from layer III. The red-legged partridge (*Alectoris rufa*) is the only common taxon to the three layers bearing fossil avian remains. In Iberia, this species is a reliable bioindicator of Mediterranean conditions (Sánchez Marco, 2004).

Taxa representing aquatic biotopes, both marine and inland, are absent, despite the coast being very close to the cave. *Columba livia* (indistinguishable from *Columba oenas*) is relatively abundant in layers I and II. This pigeon, together with *Corvus antecorax* (layer I), is a typical cave and cliff dweller. *C. antecorax* is a form related to the current common raven, *Corvus corax*, and could be regarded as a chronospecies (see Sánchez Marco, 2007). The former is of smaller size and has been found only in the Lower and Middle Pleistocene of Western Europe (Tyrberg, 1998). Other European palaeospecies of crow conform to the morphological features and approximate size of *C. antecorax*, and are apparently indistinguishable from each other; namely, *Corvus pliocaenus* (Portis, 1889), *Corvus betfianus* (Kretzoi, 1962), *C. antecorax* (Mourer-Chauviré, 1975), and *Corvus praecorax* (Depéret, 1890). Mlíkovský (2002) has synonymised *C. pliocaenus*, *C. beftianus* and *C. praecorax* with the current *Corvus corone* (carrion crow), a species of smaller size than *C. corax*. The binomen *C. antecorax* groups together crows that are somewhat larger than *C. corone* but smaller than *C. corax*.

The finding of *Plectrophenax nivalis* in layer I deserves particular mention. Currently, this bird breeds in the northern regions of Eurasia, and winters on a strip of land from northern France eastward. It is a northern irruptive species in the Mediterranean region during the Quaternary, and is linked to Pleistocene cold phases in the northern hemisphere (Sánchez Marco, 2004).

Two larks, *Galerida* sp. (*Galerida cristata* and *G. theklae* are indistinguishable) and *Calandrella brachydactyla*, occur in layer I. Both inhabit open country, namely grasslands. *Calandrella brachydactyla* has a current status of breeding species in Europe (summer visitor). The other lark is resident in the Iberian Peninsula throughout the year. The rest of the avian species are tied to woodland, parkland, shrubs and thickets. *Turdus* sp. and *Fringilla coelebs* are present in layers I and II. *Picus viridis* and *Luscinia* cf. *megarhynchos* appear only in layer II. The latter is the only species of *Luscinia* within the current Iberian avifauna that has the status of breeder. In layer I, *Parus major*, *Loxia curvirostra* and *Pyrrhula pyrrhula* represent the forest group of species, together with *F. coelebs*. *Loxia curvirostra* is a characteristic bird of coniferous areas. At present, the *Pyrrhula pyrrhula* Iberian range is restricted to the northern regions of the peninsula.

4.4.4. Charcoal

We have been able to recover 267 charcoal fragments from layers I and VIII. In general, the fragments are small-sized and most show important alterations that prevent taxonomic identification.

The layer I spectrum is dominated by an undetermined angiosperm; *Prunus* and *Rhamnus/Phillyrea* are present. There are also many undetermined fragments and charcoal particles (Table 7). Only 26 fragments were recovered from layer VIII, and most of these were undeterminable.

The available charcoal results show a dominance of angiosperms and a scarcity of conifers, which suggests a temperate environment.

4.4.5. Phytoliths

Phytoliths were identified in low numbers both in sediments (#55 and #56) and dental samples (#48 to #54). The low number of microremains in the latter was expected, since phytoliths are usually not documented in large numbers in dental calculus (Lalueza et al., 1996; Piperno et al., 2006; Staller and Thompson, 2002). The descriptions of the analysed samples, as well as the main results obtained from the study, are listed in Table 8. Six tooth samples could not be analysed due to the total dissolution of the material recovered after the first treatment with 1N HCl.

The one sample analysed from *Haploidoceros mediterraneus* (#48a) showed few phytoliths and no starches. The identified phytoliths correspond mostly to short cells characteristic of C3 pooid grasses, common in the Mediterranean, and bulliform parallelepipeds formed in the leaves of the same family (Table 8).

Table 7
Results of the charcoal analyses from Cova del Rinoceront.

Taxa	Layer I	Layer VIII
Prunus	4	
cf. *Prunus*	2	
Rhamnus/Phillyrea	1	
Undetermined angiosperm	55	1
Undetermined conifer	3	
Undetermined fragments	32	10
Charcoal particles	139	15
Total	**241**	**26**

Table 8
List of pytholith samples and analytical results. For 48a-d, the results of the phytoliths embedded in the non-dissolved calculus are shown between brackets.

Sample ID	Site#	Layer	Material	Taxon and tooth	Part	% AIF	# Phytoliths identified	# phytoliths per 1 g of AIF	# starches identified	Plant attribution
48a	1364a	I	Tooth	*H. mediterraneus*	P_2 left	67.8	4	7000	0	Grasses (bulliform and short cell rondels common in C3 pooideae grasses)
48b	1364b	I	Tooth	*H. mediterraneus*	P_2 left	No material recovered				
49	1380	I	Tooth	*H. mediterraneus*	Lower different teeth	No material recovered				
50	569	I	Tooth	*H. mediterraneus*	Lower different teeth	No material recovered				
51	3292	I	Tooth	*H. mediterraneus*	Lower different teeth	No material recovered				
52a	3124a	I	Tooth	*C. elaphus*	P_3 right	66.3	0 (15)	0 (30,000)	0	Grasses (short cells rondel common in C3 pooideae grasses), dicot wood/bark and leafs
52b	3124b	I	Tooth	*C. elaphus*	M_1 right	65.5	4 (35)	8000 (72,000)	2	Grasses (short cells rondel common in C3 pooideae grasses), dicot wood/bark
52c	3124c	I	Tooth	*C. elaphus*	M_3 right	45.6	1 (47)	2000 (113,000)	1	Grasses (short cells rondel common in C3 pooideae grasses), dicot wood/bark, monocots, dicot leaves
52d	3124d	I	Tooth	*C. elaphus*	P_2-M_3 right	54.4	1 (22)	2000 (36,000)	14	Grasses (Short cells rondel common in C3 pooideae grasses), dicot wood/bark
53	2500	I	Tooth	*C.* cf. *ibex*	Lower different teeth	No material recovered				
54	1335	Rubble-III	Tooth	*S. hundsheimensis*	M_3	83.9	0	0	65	No phytoliths recovered
55	8021	I	Sediment			58.5	0	0	0	No phytoliths recovered
56	8022	I	Sediment			76.8	1	22	0	Grasses (short cell rondel common in C3 pooideae grasses)

The calculus from *C. elaphus* (#52) was not easily dissolved and most of the phytoliths from sample P_3 (#52a) were embedded in the calculus. The isolated phytoliths identified in M_1 (#52b) and M_3 (#52c) correspond mostly to spheroids and parallelepiped thins from the wood/bark of dicotyledonous plants (Table 8), as well as to bulliform cells and short cells from grasses. Interestingly, the phytoliths embedded in the calculus showed a much richer morphological diversity, with phytoliths from grasses, wood/bark of trees and hairs of the unciform type, commonly found in the leaves of the *Leguminosae* family. This latter finding is especially interesting since hairs are not usually found in sediments due to post-depositional processes.

Some current studies of peninsular *C. elaphus* show that the main diet is grasses during spring and summer, while dicotyledonous consumption is highest during fall and winter (Mitchell et al., 1977). Leguminous shrub consumption is characteristic of the population of deer in the Mediterranean area, especially during the spring season (Álvarez and Ramos, 1991; Garin et al., 2001).

The starches recovered from this individual were characteristic of the seeds of the grass family. Thus, the results suggest that, the *C. elaphus* individual (#52) would consume grasses and leaves of the *Leguminosae* family probably during the spring season.

The rhino sample (#54) showed the highest amount of starches (Table 8) but did not contain phytoliths. Morphologically, the starches seem to correspond mostly to grasses with few exceptions. Polygonal shapes resemble those from the C4 panicoid subfamily grass, which is characteristic of temperate and wet environments (Yang et al., 2012; Yang and Perry, 2013). This interpretation should be taken with caution since more reference samples from Mediterranean grasses need to be analysed to test it.

Several studies show that rhino species are adapted to their environmental conditions and their diet varies according to local factors (availability of grasses, bushes, woody plants, leaf, fruits, bark; Kahlke and Kaiser, 2011). It is thought that hypsodonty is an adaptation to abrasive diets (Strömberg et al., 2007), which would support the consumption of grasses by this individual.

The poor preservation of phytoliths in the sediment samples was probably related to the terra rossa soil (Albert et al., 1999) and the high alkalinity associated with a more or less constant flux of water. The few phytoliths identified correspond to short cell rondels, which are characteristic of the C3 Pooideae subfamily. The low presence of phytoliths in the sediment samples prevents a detailed vegetation reconstruction.

5. Synthesis and discussion

5.1. Chronology

The 11 m-thick sedimentary sequence of Cova del Rinoceront was deposited over a relatively broad temporal range, spanning the late Middle Pleistocene and the beginning of the Upper Pleistocene. The chronological range of the sequence is provided basically by the U–Th results. The capping flowstone gives a minimum age for the deposit of ~84 ka and the maximum age is provided by a speleothem from layer VII (~175 ka). The chronostratigraphic interpretation of the sequence is (a) speleothem formation on cave walls occurs in MIS 7, (b) accumulation of Unit 3 (prior to cave opening) and Unit 2 (after the cave opened) in MIS 6, and, finally, (c) deposition of Unit 1 in MIS 5.

The luminescence, AAR and ESR ages provide further chronological constraints on the infill phases and enable multi-technique assessments of dating consistency. A comparison of the TL results obtained for the two samples from layer I shows good agreement, yielding a combined age of 87 ± 5 ka. The ages for layer II show reasonable consistency between the different dating methods: the IRSL sample from this layer provides an age of 104 ± 8 ka, an ESR sample from the same depth provides an age of 93 ± 7 ka, and the mean age obtained from the amino acid sample is 99 ± 22 ka.

Layer III has two IRSL ages that are statistically indistinguishable (128 ± 9 and 129 ± 10 ka) and consistent with the various amino acid results (between 126 ± 34 to 142 ± 46 ka). The U–Th ages on two small cement-filled cracks (#4 and 5) are not considered to be representative because they could be developed during the uppermost flowstone formation. The U-series date on an elephant tusk (sub-layer IIIc) suggests an age of ~95 ka, although without means to judge U uptake this may represent a minimum age, while

two rhinoceros bone samples coming from ~40 cm below provide maximum ages of 133.6 and 147 ka, consistent with the IRSL ages. The IRSL age for layer V is consistent with these U-series results. The sample from the top of this layer gives an IRSL age of 144 ± 10 ka, while the amino acids from the same depth are dated to 144 ± 38 ka. Though the precision of this amino acid ages is low, they are supported by two additional, stratigraphically consistent amino acid ages of 165 ± 23 ka and 209 ± 79 ka towards the base of layer V. These AAR results are consistent with an MIS 6 age for layers VII-VIII.

5.2. Palaeoenvironmental reconstruction

Three different components can be recognised in the Cova del Rinoceront palaeontological assemblage: a) human activity, as indicated by washed-in artefacts; b) carnivore activity, as evidenced by coprolites, carnivore and herbivore remains and gnawing damage; and c) natural pit-fall trap accumulations, as determined by articulated carcasses without subsequent damage/exploitation. The evidence for human activity is relatively scarce and the recovered charcoal likely corresponds to wildfires rather than campfires. However, the documented stone tools clearly point to some human presence in another area of the cave or outside. Cova del Rinoceront is therefore another example of a Middle and early Upper Pleistocene palaeontological site yielding scant evidence of human activity, in spite of a well-defined regional archaeological context (Brugal and Jaubert, 1991). Such sites are characterised by high amounts of faunal remains, most corresponding to natural formation processes, and residual remains of human activity in the form of some lithic artefacts and cut-marked bones. Human presence can be attributed to short-term visits that did not entail residential occupation of the caves or of the areas surrounding their entrances. Such assemblages are well represented in NW Iberia and have been identified at the nearby, early Upper Pleistocene sites of Cova del Gegant (Daura et al., 2005) and Cova de les Teixoneres (Tissoux et al., 2006). Carnivores are likely the main agents responsible for carcass modification in Units 1 and 2 (Sanz, 2013). The taphonomic features of the bones, including the presence of articulated elements, low levels of long-bone reduction, the presence of non-hyena coprolites, the absence of partly digested bones and the dominance of medium-sized deer, suggest the agent involved is either a canid or a felid – the latter could also be consistent with secondary access by canids, which would have disguised the felid signature. A natural death for many of the individuals, especially for the middle and lower layers, cannot be ruled out. In fact, the complete Proboscidean skeleton (sub-layer IIIc), which does not display carnivore damage, could have been the victim of a natural pit-fall trap. Preliminary taphonomic analysis on the tortoise specimens from sub-layers IIIa-IIIb suggests a similar natural accumulation process.

Ascertaining connections between past climate and faunal records from karstic traps can be complex, and requires careful consideration of formation processes. At Cova del Rinoceront, the apparent physical association of several types of remains could be misleading, and is likely attributable to bias induced by slope wash mode of accumulation.

The palaeovegetation record of Cova del Rinoceront, though limited, is indicative of temperate environmental conditions, as is the scarcity of conifers. Overall, the phytolith and charcoal analyses reveal mixed wooded vegetation and open areas dominated by grasses and other dicotyledonous herbaceous plants that are characteristic of temperate Mediterranean climates, such as *Leguminosae*. Similar environmental and climatic conditions are indicated for the upper part of the sequence by the small-vertebrate assemblages. The microfaunal taxa are characteristic of a landscape dominated by open forest areas and mild climatic conditions, perhaps slightly more humid than today.

The Iberian palaeobotanical sequences for this period suggest overall mild climatic conditions and a diversity of landscapes, with temperate taxa distributed according to biogeographical location. The Cova del Rinoceront data are according to palynological records indicative of the importance of mesothermofillous taxa with *Quercus* and Oleaceae (González-Sampériz et al., 2010, 2013; Carrión, 2012), as recorded in Padul (720 m amsl) and La Carihuela cave (1020 m amsl). However, closer to the Mediterranean Sea, as in the Alfaix travertine platform (105 m amsl), the above mentioned vegetation is present together with decidous oaks and xerophile species (Schulte et al., 2008). In interior Iberia, the higher values of conifers suggest more arid environments (González-Sampériz et al., 2013), while the Pla del Estany (zone B) sequence shows a dominance of arboreal taxa indicating milder and more humid climatic conditions above 42° latitude (Carrión, 2012); however, the latter's assignment to MIS 5 is uncertain.

The large mammal records for layers I (sub-layers Ic and Ie) and II are notable for the absence of species adapted to open environments, such as horse, and the scarcity of bovids, together with the presence of *Capra*. The small mammals might also be indicative of a temperate, wooded, mountainous environment. Although the habitat of the *Haploidoceros* deer is unknown, Croitor et al. (2008) suggested that it corresponded to an open environment with hard forage, which is typical of an arid climate. Indeed, the *Haploidoceros* deer found in the Lunel Viel assemblage is associated with forest and open landscape taxa, as are the large bovids (*Bos primigenius*) and horses (*Equus mosbachensis* and *E. hydruntinus*), red deer (*C. elaphus*), rhinoceroses (*Stephanorhinus etruscus*) and wild boar (*Sus scrofa*). A similar faunal record is documented at Igue des Rameaux, and is complemented by the presence of tahr (*Hemitragus bonali*), elephant (*E. antiquus*) and woolly rhinoceros (*Coleodonta antiquitatis*) (Rouzaud et al., 1990).

The dominance of deer in fossil assemblages is documented at other Iberian sites such as Cueva del Camino (Pinilla del Valle), dated to ~90 ka (Arsuaga et al., 2012). *Haploidoceros has not been* identified at the site, but fallow deer is the most abundant taxa, together with other forest species, such as roe deer or wild boar (Álvarez-Lao et al., 2013), followed by open landscape taxa, such as horses, bovids and rhinoceroses (Álvarez-Lao et al., 2013).

Among the birds, the presence of *Plectrophenax nivalis* in sublayer Ig, in association with forest dwellers, together with the sedimentological features of this unit (gravels without a clay matrix), indicates a cold phase during MIS 5, with coniferous woodland landscapes.

The faunal composition of layers I, II and III indicates widespread temperate conditions. In particular, the Mediterranean tortoise, *T. hermanni*, is a key warm climatic indicator (García and Arsuaga, 2003) and is present at other Iberian sites (Morales and Sanchís, 2009). Tortoises need warm temperatures for their survival, with suitable temperatures ranging from 20 °C to 25 °C in sunlight and no lower than −5 °C during hibernation. Critically, the condition required for egg-laying is a soil temperature of around 30 °C. Mid-high humidity is also needed not only for reproduction but also for the survival of pregnant females (Nabais, 2010). The high number of tortoise remains in layer III (sub-layers IIIa to IIIc) is therefore indicative of a warmer episode and could perhaps be related to MIS 5e. However we cannot exclude that this concentration reflects sample bias or a particular taphonomical process. The ages obtained for layer III are consistent with an attribution of these sublayers to MIS 5e, as they range between 119 and 140 ka.

In contrast, the presence of several rhinoceros remains in sublayer IIIe points to an open landscape. This suggests a drier environment and probably hard forage, as evidenced by tooth wear. It is

possible, therefore, that layer sub-layer IIIe corresponds to the boundary between MIS 5e and MIS 6. In the Mediterranean latitudes, it is difficult to ascertain whether the disappearance of woody environments is the result of an aridity crisis related to an extreme cold event. Arctic and steppe elements are absent or rare in the fossil record (García and Arsuaga, 2003), and the presence of a cold-adapted fauna at the end of MIS 6 is rare across Iberia. The only unambiguous evidence of *Coelodonta antiquitatis* in association with *Rangifer tarandus* in the Iberian MIS 6 record, suggesting an open, dry and cold steppe-tundra environment, comes from La Parte (Asturias), dated to ~150 ka (Álvarez-Lao and García, 2006).

5.3. Implications for MIS 5 reconstruction in the Iberian Peninsula

During the Upper Pleistocene, increasingly abrupt climatic fluctuations continued up until the LGM. The last mild phase corresponds to the interval from the beginning of the MIS 5e/Eemian to the end of MIS 5a, represented at Cova del Rinoceront by layers I to III. In the Iberian Peninsula, some scholars (Álvarez-Lao et al., 2013) have attempted to correlate individual stratigraphic units to MIS 5 climatic sub-stages; however, the available chronological evidence is seldom precise enough to reconstruct such climate changes inland. Moreover, palaeoecological correlations between deep sea or ice cores and short land sequences are typically imprecise because stratigraphic layers from cave traps could potentially correspond to palimpsests.

The most significant feature of the Cova del Rinoceront MIS 5 sequence is the presence of species that were previously only known in older (Lower or Middle Pleistocene) sites of the Mediterranean region, such as the cervid *Haploidoceros mediterraneus*, the corvid *C. antecorax*, and, potentially, the rhinoceros, if assignment to *S. hundsheimensis* is confirmed by future analyses. The presence of these species could point to a problem of taxonomic identification in previous studies because fossil remains are usually fragmentary and often lack diagnostic elements. It may also be an outcome of sampling bias. MIS 5 sites along the Mediterranean margin are too scarce to evaluate whether this persistence is genuinely the result of the Iberian Peninsula housing an isolated refugium until MIS 5, or whether these taxa were more widespread than hitherto thought. Similarly, the presence of the fat dormouse (*Glis glis*) prior and up to MIS 5 at Cova del Rinoceront alone could be the result of the taxon's limited representation during these periods or may reflect an under-representation of MIS 5 sites in the Iberian Peninsula.

C. antecorax is well documented from the Late Pliocene to Middle Pleistocene. In France, this taxon has been found from the Late Pliocene site of Saint Valière to the Middle Pleistocene sites of La Fage, Lazaret (Locus VIII) and Orgnac 3 (Mourer-Chauviré, 1975; Tyrberg, 1998; Sánchez Marco, 2004). The earliest record of this extinct crow in Spain is from the Late Pliocene site of Las Higueruelas (Sánchez Marco, 2004, 2005), and it has also been documented at the Early Pleistocene site of Cueva Victoria (Sánchez Marco, 2004) and the Early and Middle Pleistocene layers of the Atapuerca complex (Sánchez Marco, 1987, 1995, 1999a, 1999b), as well as in the Middle Pleistocene layers of Gruta da Aroeira (Galerias Pesadas, Almonda karstic system; Trinkaus et al., 2003). However, this palaeospecies had not yet been found in European Late Pleistocene sites (Tyrberg, 1998).

The osteological and metrical parameters of the *Haploidoceros mediterraneus* from Cova del Rinoceront overlap with other species of deer, mainly *Dama dama* (Sanz et al., 2014). This small to medium sized deer was present from MIS 9 to MIS 7 in the South of France (Croitor et al., 2008); however, the age of the deposits at Lunel-Viel and Igue-des-Rameaux is based on biochronology, not on absolute dating. The numerical chronology established at Cova del Rinoceront firmly demonstrates the existence of this species until MIS 5 in the Iberian Peninsula.

The preliminary study of rhinoceros remains does not permit accurate taxonomic determination due to the broad affinities between *S. etruscus* and *S. hundsheimensis*. Given the Late Pleistocene age of Cova del Rinoceront, the occurrence of the species *S. etruscus* would be unexpected as this species is thought to have been long extinct at this time in western Europe. However, the unquestionable presence of the cervid *Haploidoceros mediterraneus*, a taxon previously undocumented beyond ~350 ka if the chronology of Lunel-Viel is correct, as cautioned above, does not rule out the presence of *S. etruscus* at this site. *S. hundsheimensis* is commonly present in other areas until ~500 ka (van der Made, 2010); even so, its occurrence at Cova del Rinoceront would contradict existing age ranges. A more detailed comparative study of the rhinoceros remains may allow a more precise taxonomic assessment. We must also note that the rhinoceros remains have been directly dated by U–Th to 135 ka, a time range when Iberian rhinoceros remains are mainly assigned to the species *S. hemitoechus* (van der Made, 2010).

The presence of *Capra* cf. *ibex* at Cova del Rinoceront is significant because until now it has not been identified in and south of the Pyrenees foothills. The cranial morphology suggests a non *C. caucasica*- *Capra pyrenaica* lineage, as could be inferred from the geographical and chronological ranges previously proposed for species of this genus (Crégut-Bonnoure, 1992, 2009). In fact, several osteological differences can be noted between the two lineages (Crégut-Bonnoure, 2009), although genetic evidence suggests a common origin for *C. pyrenaica* and *C. ibex* from a primitive lineage, followed by isolation of the latter in the Iberian Peninsula during the Last Glacial (Manceau et al., 1999; Ureña et al., 2011). However, morphological and genetic comparison studies of *C. pyrenaica* and *C. ibex* suggest that the taxonomy of *Capra* spp. must be revised (Ureña et al., 2011).

The presence of *Glis glis* in the lower part of the Cova del Rinoceront sequence (layer VII) represents one of the oldest documented occurrences of this species in the Iberian Peninsula. Prior to this study, *Glis glis* was only reported from the latest Pleistocene to early Holocene (40–3 ka) archaeo-palaeontological record of northern and northeastern Iberia. The first documented *Glis glis* remains date to around 40 ka at sites such as Gabasa, Labeko Koba or Teixoneres caves, where their context suggests temperate and humid conditions and a landscape characterised by some tree cover. This species became most abundant after 20 ka, as shown by the cave sites of l'Arbreda, La Riera, El Mirón, Pendo, El Rascaño, Laminak II, Valdavara-1 or Toll, among others (López-García, 2011; López-García et al., 2012; Fernández-García and Fernández-García, 2014). However, *Glis glis* is known in the French late Middle Pleistocene sites of l'Arago, Lazaret and Moula-Guerçy, which have MIS 13 and MIS 6 ages (Hanquet, 2011); therefore, the presence of this species at Cova del Rinoceront indicates that this taxon in Iberia goes back to the Middle Pleistocene, which extends its previously recorded temporal range.

6. Conclusion

Upper Pleistocene terrestrial bioarchaeological archives have traditionally been difficult to date beyond the limits of radiocarbon dating. We demonstrate here the advantages of undertaking a multi-technique dating comparison at such sites. U-series, TL, IRSL, ESR and amino acid ages obtained on the MIS 5 to MIS 6 Cova del Rinoceront sequence are in good agreement and enable us to place robust chronological constraints on the fossil deposits.

Layers I to III of the Cova del Rinoceront sequence provide one of the most continuous and complete MIS 5 terrestrial records of the Mediterranean region. The most significant novelties of the Cova

del Rinoceront assemblage include the earliest occurrence of *Glis glis* in the Iberian Peninsula and the presence of *Haploidoceros*, *Stephanorhinus hundsheimensis* and *C. antecorax*, previously identified only in Early or Middle Pleistocene localities. The younger than expected occurrence of these species at Cova del Rinoceront may be explained by one of four hypotheses: (1) these species genuinely persisted until the Upper Pleistocene in this region, (2) the chronological assignments of these species at other localities are unreliable or derived from faunal associations of uncertain age (indeed, several of the sites used as the basis of past biochronological schemes do not have independent age controls), (3) there are problems of reliable taxonomic identification when dealing with fragmentary remains, and (4) the limited number of preserved and accessible palaeontological sites have biased previous biochronological age assignments. From this study, two conclusions are clear: extensive chronometric dating of Middle to Late Pleistocene palaeontological sites should be considered a research priority; the utility of some biostratigraphical indicators and, hence, the validity of existing assessments of the chronological distribution of some species should be considered with caution.

Acknowledgements

This paper is an output of the archaeological research project *El Plistocè Superior a la costa central catalana: paleoambients i ocupació dels neandertals* (2014/100639) sponsored by Servei d'Arqueologia i Paleontologia – Generalitat de Catalunya (G.C.) and Castelldefels City Council. Sampling and laboratory analyses were funded by Catalan (2014SGR-00108) and Spanish (HAR2011-26193, HAR2011-26193, CGL2010-18616, CGL2012-38358, CGL2012-38434-C03-03 and CGL2013-48441-P) MICINN Projects. J. Daura has been supported by a postdoctoral grant (Juan de la Cierva Subprogram JCI-2011-09543), J.M. López-García by a postdoctoral fellowship (2011BP-A00272) from the G.C. a grant co-funded by the European Union through the Marie Curie Actions of the 7th Framework Program for R + D. We are also grateful to R. Álvarez (UB) for lithics' photos. J. Mangope, Williams College, prepared and measured the ESR sample. D. Lawrence, Wadsworth Laboratories of the New York State Public Health Service provided access to the source for the ESR irradiations. Funding for the ESR spectrometer came from NSF grant ILI 9151111; other funding was provided by Williams College. L. Arnold and M. Demuro were supported by MINECO grant CG2010-16821, Australian Research Council Future Fellowship F130100195, and Marie Curie International Reintegration grant PIRG08-GA-2010-276810. Thanks to the Paleomagnetism Laboratory of Barcelona (CCiTUB-CSIC) where the paleomagnetic analyses were carried out.

References

Aitken, M.J., 1985. Thermoluminescence Dating. Academy Press, London.
Aitken, M.J., 1998. An Introduction to Optical Dating: the Dating of Quaternary Sediments by the Use of Photon-stimulated Luminescence. Oxford University Press, Oxford.
Albert, R.M., Esteve, X., Portillo, M., Rodríguez-Cintas, A., Cabanes, D., Esteban, I., Hernández, F., 2011. Phytolith CoRe, Phytolith Reference Collection. Retrieved [April 2013], from. http://www.gepeg.org/enter_PCORE.html.
Albert, R.M., Lavi, O., Estroff, L., Weiner, S., Tsatskin, A., Ronen, A., Lev-Yadun, S., 1999. Mode of occupation of Tabun Cave, Mt Carmel, Israel during the Mousterian period: a study of the sediments and phytoliths. J. Archaeol. Sci. 26, 1249–1260.
Almera, J., 1898. Compte-rendu de l'excursion du Jeudi, 6 Octobre à Castelldefels et costes de Garraf. B. Soc. Geol. Fr. 26, 801–811.
Álvarez, G., Ramos, J., 1991. Estrategias alimentarias del ciervo *(Cervus elaphus L.)* en Montes de Toledo. Doñana. Acta Vertebr. 18, 63–99.
Álvarez-Lao, D.J., 2007. Revisión paleontológica de los macromamíferos indicadores de clima frío en el Pleistoceno de la Península Ibérica (Ph.D. thesis). Univ. Oviedo.
Álvarez-Lao, D.J., García, N., 2006. A new site from the Spanish Middle Pleistocene with cold-resistant faunal elements: la Parte (Asturias, Spain). Quat. Int. 142–143, 107–118.
Álvarez-Lao, D.J., Arsuaga, J.L., Baquedano, E., Pérez-González, A., 2013. Last Interglacial (MIS 5) ungulate assemblage from the Central Iberian Peninsula: the Camino Cave (Pinilla del Valle, Madrid, Spain). Palaeogeogr. Palaeoclimatol. Palaeoecol. 374, 327–337.
Ambrosetti, P., 1972. Lo scheletro di *Dicerorhinus etruscus* (FALCONER, 1868) di Capitone (Umbria meridionale). Geol. Romana 11, 177–198.
Arnold, L.J., Roberts, R.G., 2009. Stochastic modelling of multi-grain equivalent dose (D_e) distributions: implications for OSL dating of sediment mixtures. Quat. Geochronol. 4, 204–230.
Arnold, L.J., Roberts, R.G., 2011. Paper I – optically stimulated luminescence (OSL) dating of perennially frozen deposits in north-central Siberia: OSL characteristics of quartz grains and methodological considerations regarding their suitability for dating. Boreas 40, 389–416.
Arnold, L.J., Bailey, R.M., Tucker, G.E., 2007. Statistical treatment of fluvial dose distributions from southern Colorado arroyo deposits. Quat. Geochronol. 2, 162–167.
Arnold, L.J., Demuro, M., Navazo Ruiz, M., 2012. Empirical insights into multi-grain averaging effects from 'pseudo' single-grain OSL measurements. Radiat. Meas. 47, 652–658.
Arnold, L.J., Roberts, R.G., MacPhee, R.D.E., Haile, J.S., Brock, F., Möller, P., Froese, D.G., Tikhonov, A.N., Chivas, A.R., Gilbert, M.T.P., Willerslev, E., 2011. Paper II – dirt, dates and DNA: OSL and radiocarbon chronologies of perennially frozen sediments in Siberia, and their implications for sedimentary ancient DNA studies. Boreas 40, 417–445.
Arsuaga, J.L., Baquedano, E., Pérez-González, A., Sala, M.T.N., García, N., Álvarez-Lao, D., Laplana, C., Huguet, R., Sevilla, P., Blain, H.-A., Quam, R., Ruiz Zapata, M.B., Sala, P., Gil García, M.J., Uzquiano, P., Pantoja, A., 2010. El yacimiento kárstico del Pleistoceno Superior de la Cueva del Camino en el Calvero de la Higuera (Pinilla del Valle, Madrid). Zona Arqueol. 13, 349–368.
Arsuaga, J.L., Baquedano, E., Pérez-González, A., Sala, N., Quam, R.M., Rodríguez, L., García, R., García, N., Álvarez-Lao, D.J., Laplana, C., Huguet, R., Sevilla, P., Maldonado, E., Blain, H.A., Ruiz-Zapata, M.B., Sala, P., Gil-García, M.J., Uzquiano, P., Pantoja, A., Márquez, B., 2012. Understanding the ancient habitats of the last-interglacial (late MIS 5) Neanderthals of central Iberia: paleoenvironmental and taphonomic evidence from the Cueva del Camino (Spain) site. Quat. Int. 275, 55–75.
Asmerom, Y., Polyak, V.J., Burns, S.J., 2010. Variable winter moisture in the southwestern United States linked to rapid glacial climate shifts. Nat. Geosci. 3, 114–117.
Auclair, M., Lamothe, M., Huot, S., 2003. Measurement of anomalous fading for feldspar IRSL using SAR. Radiat. Meas. 37, 487–492.
Ayarzagüena, J., López Martínez, N., 1976. Estudio filogenético y comparativo de *Microtus cabrerae* y *Microtus brecciensis*. Doñana. Acta Vertebr. 3, 181–204.
Bar-Matthews, M., Ayalon, A., Gilmour, M., Matthews, A., Hawkesworth, C.J., 2003. Sea–land oxygen isotopic relationships from planktonic foraminifera and speleothems in the Eastern Mediterranean region and their implication for paleorainfall during interglacial intervals. Geochim. Cosmochim. Acta 67, 3181–3199.
Barnosky, A.D., Koch, P.L., Feranec, R.S., Wing, S.L., Shabel, A.B., 2004. Assessing the causes of Late Pleistocene extinctions on the Continents. Science 306, 70–75.
Berger, G.W., Pérez-González, A., Carbonell, E., Arsuaga, J.L., Bermúdez de Castro, J.M., Ku, T.L., 2008. Luminescence chronology of cave sediments at the Atapuerca paleoanthropological site, Spain. J. Hum. Evol. 55, 300–311.
Bischoff, J.L., Fitzpatrick, J.A., 1991. U-series dating of impure carbonates: an isochron technique using total-sample dissolution. Geochim. Cosmochim. Acta 55, 543–554.
Blain, H.-A., Laplana, C., Sevilla, P., Arsuaga, J.L., Baquedano, E., Pérez-González, A., 2014. MIS 5/4 transition in a mountain environment: herpetofaunal assemblages from Cueva del Camino, central Spain. Boreas 43, 107–120.
Blain, H.-A., López-García, J.M., Cuenca-Bescós, G., 2011. A very diverse amphibian and reptile assemblage from the late Middle Pleistocene of the Sierra de Atapuerca (Sima del Elefante, Burgos, Northwestern Spain). Geobios 44, 157–172.
Blain, H.-A., Panera, J., Uribelarrea, D., Rubio-Jara, S., Pérez-González, A., 2012. Characterization of rapid climate shift at the MIS 8/7 transition in central Spain (Valdocarros II, Autonomous Region of Madrid) by means of herpetological assemblages. Quat. Sci. Rev. 47, 73–81.
Blasco, R., 2008. Human consumption of tortoises at layer IV of Bolomor Cave (Valencia, Spain). J. Archaeol. Sci. 35, 2839–2848.
Boeuf, O., 1995. Le *Dicerorhinus etruscus* (Rhinocerotidae, Mammalia) du site pliocène supérieur de Chilhac (Haute-Loire, France). Geobios 28, 383–391.
Bona, F., Sala, B., Tontori, A., 2008. Early toringian small mammal fauna from Fontana Marella cave (Varese, Lombardy, North Italy). Riv. Ital. Paleontol. S. 114, 133–144.
Bosch, R.F., White, W.B., 2004. Lithofacies and transport of clastic sediments in karstic aquifers. In: Sasowsky, I.D., Mylroie, J. (Eds.), Studies of Cave Sediments. Physical and Chemical Records of Paleoclimate. Kluwer Academic/Plenum Publishers, New York, pp. 1–22.
Boyadjian, C.H.C., Eggers, S., Reinhard, K., 2007. Dental wash: a problematic method for extracting microfossils from teeth. J. Archaeol. Sci. 34, 1622–1628.
Brugal, J.-Ph, Jaubert, J., 1991. Les gisements paléontologiques pléistocènes à indices de frequentation humaine: un nouveau type de comportement de prédation? Paléo 3, 15–41.

Burke, A., Eisenmann, V., Ambler, G.K., 2003. The systematic position of *Equus hydruntinus*, an extinct species of Pleistocene equid. Quat. Res. 59, 459–469.
Carrión, J.S., 2012. Paleoflora y Paleovegetación de la Península Ibérica e Islas Baleares: Plioceno-Cuaternario. Ministerio de Economía y Competitividad-Univ. Murcia, Murcia.
Channell, J.E.T., 2006. Late Brunhes polarity excursions (Mono Lake, Laschamp, Iceland Basin and Pringle Falls) recorded at ODP site 919 (Irminger Basin). Earth Planet. Sc. Lett. 244, 378–393.
Cheng, H., Edwards, R.L., Shen, C.-C., Polyak, V.J., Asmerom, Y., Woodhead, J., Hellstrom, J., Wang, Y., Kong, X., Spötl, C., Wang, X., Alexander Jr., E.C., 2013. Improvements in ^{230}Th dating, ^{230}Th and ^{234}U half-life values, and U-Th isotopic measurements by multi-collector inductively coupled plasma mass spectrometry. Earth Planet. Sc. Lett. 371-372, 82–91.
Crégut-Bonnoure, E., 1992. Intérêt biostratigraphique de la morphologie dentaire de *Capra* (Mammalia, Bovidae). Ann. Zool. Fenn. 28, 273–290.
Crégut-Bonnoure, E., 2005. Nouvelles données paléogéographiques et chronologiques sur les *Caprinae* (Mammalia, Bovidae) du Pléistocène moyen et supérieur d'Europe. Munibe (Antropologia-Arkeologia) 57, 205–219.
Crégut-Bonnoure, E., 2009. Biochronologie et grands mammifères au Pléistocène moyen et supérieur en Europe occidentale: l'apport des genres *Hemitragus* et *Capra*. Quat 20, 481–508.
Crégut-Bonnoure, E., Boulbes, N., Daujeard, C., 2010. Nouvelles donnés sur la grande faune de l'éemien dans le sud-est de la France. Quaternaire 21, 227–248.
Croitor, R., Bonifay, M.-F., Brugal, J.-Ph, 2008. Systematic revision of the endemic deer Haploidoceros n. Gen. Mediterraneus (BONIFAY, 1967) (Mammalia, Cervidae) from the Middle Pleistocene of Southern France. Paläontol. Z. 82 (3), 325–346.
Currant, A., Jacobi, R., 2001. A formal mammalian biostratigraphy for the Late Pleistocene of Britain. Quat. Sci. Rev. 20, 1707–1716.
Daura, J., 2008. Caracterització arqueològica i paleontològica dels jaciments plistocens del massís del Garraf-Ordal i curs baix del riu Llobregat (Ph.D. thesis). Univ. Barcelona.
Daura, J., Sanz, M., Vaquero, M., 2005. El Pleistoceno de la Cova delRinoceront (Castelldefels, Barcelona). In: Ferreira-Bicho, N. (Ed.), O Paleolítico. Actas do IV Congresso de Arqueologia Peninsular, Promontoria Monográfica 2, pp. 217–227.
Daura, J., Sanz, M., Font, O., Budó, J., 2006. Restes fòssils de *Testudo hermanni* al massís del Garraf. Butll. Soc. Catalana d'Herpetol. 17, 9–20.
Daura, J., Sanz, M., Rosell, J., Julià, R., 2010. Un cubil de carnívoros delPleistoceno medio y superior con escasa presencia humana: la Cova del Rinoceront (Castelldefels, Barcelona). In: Baquedano, E., Rosell, J. (Eds.), Actas de la 1ª reunión de científicos sobre cubiles de hiena (y otros grandes carnívoros) en los yacimientos arqueológicos de la Península Ibérica, Zona Arqueológica 13, pp. 494–499.
Daura, J., Sanz, M., García, N., Allue, E., Vaquero, M., Fierro, E., Carrión, J.S., López-García, J.M., Blain, H.-A., Sánchez-Marco, A., Valls, C., Albert, R.M., Fornós, J.J., Julià, R., Fullola, J.M., Zilhão, J., 2013. Terrasses de la Riera dels Canyars(Barcelona, Spain): the landscape of Heinrich Event 4 north of the "Ebro frontier" and implications for modern human dispersal into Iberia. Quat. Sci. Rev. 60, 26–48.
Daura, J., Sanz, M., Fornós, Asensio, A., Julià, R., 2014. Karst evolution of the Garraf Massif (Barcelona, Spain): doline formation, chronology, and archaeo-paleontological archives. J. Caves Karst Stud. 76, 69–87.
Desclaux, E., 1992. Les petits vertébrés de la Caune de l'Arago. Paléontologie, paléoécologie et taphonomie (Ph.D. thesis). M.N.H.N., Paris.
Falguères, Ch, Yokoyama, Y., Arrizabalaga, A., 2005. La Geocronología del yacimiento pleistocénico de Lezetxiki (Arrasate, País Vasco). Crítica de las dataciones existentes y algunas nuevas aportaciones. Munibe (Antropologia-Arkeologia) 57, 93–106.
Fernández-García, M., 2014. Paleoecología y biocronología mediante el estudio de los roedores del Pleistoceno Superior-Holoceno de la cueva del Toll (Moià, Cataluña, NE de la península Ibérica). Treb. Mus. Geol. Barc. 20, 73–97.
Fernández-García, M., López-García, J.M., 2013. Palaeoecology and biochronology based on the rodents analysis from the Late Pleistocene/Holocene of Toll Cave (Moià, Barcelona). Span. J. Palaeontol. 28, 227–238.
Fernández-Peris, J., 2007. La Cova del Bolomor (Tavernes de la Valldigna, Valencia). Las indutrias líticas del Pleistoceno Medio en el ámbito Peninsular. In: Servicio de Investigación Prehistórica, Serie de Trabajos Varios 108. Valencia.
Fernández-Peris, J., Barciela, V., Blasco, R., Cuartero, F., Sañudo, P., 2008. El Paleolítico Medio en el territorio valenciano y la variabilidad tecno-económica de la Cova de Bolomor. Treballs d'Arqueol. 14, 141–169.
Fortelius, M., Mazza, P., Sala, B., 1993. *Stephanorhinus* (*Mammalia-Rhinocerotidae*) of the Western Europen Pleistocene, with a revision of *S. etruscus* (Falconer, 1868). Palaeontogr. Ital. 80, 63–155.
García, N., Arsuaga, J.L., 2003. Late Pleistocene cold-resistant faunal complex: Iberian occurrences. Quaternary climatic changes and environmental crises in the Mediterranean Region. In: Reumer, J.W.F., De Vos, J., Mol, D. (Eds.), Advances in Mammoth Research (Proceedings of the Second International Mammoth Conference, Rotterdam, May 16–20 1999). Deinsea 9, pp. 159–169.
Garin, I., Aldezabal, A., García-González, R., Aihartza, J.R., 2001. Composición y calidad de la dieta del ciervo (*Cervus elaphus* L.) en el norte de la península ibérica. Anim. Biodivers. Conserv. 24, 53–63.
González-Sampériz, P., Leroy, S.A.G., Carrión, J.S., Fernández, S., García-Antón, M., Gil-García, M.J., Uzquiano, P., Valero-Garcés, B., Figueiral, I., 2010. Steppes, savannahs, forests and phytodiversity reservoirs during the Pleistocene in the Iberian Peninsula. Rev. Palaeobot. Palynol. 162, 427–457.
González-Sampériz, P., García-Prieto, E., Aranbarri, J., Valero-Garcés, B., Moreno, A., Gil-Romera, G., Sevilla-Callejo, M., Santos, L., Morellón, M., Mata, P., 2013. Reconstrucción paleoambiental del último ciclo glacial-interglacial en la Iberia continental: la secuencia del Cañizar de Villarquemado (Teruel). Cuad. Invest. Geográf. 39, 49–76.
Goodfriend, G.A., 1991. Patterns of racemization and epimerisation of amino acids in land snail shells over the course of the Holocene. Geochim. Cosmochim. Acta 55, 293–302.
Goodfriend, G.A., Meyer, V., 1991. A comparative study of the kinetics of amino acid racemization/epimerization in fossil and modern mollusc shells. Geochim. Cosmochim. Acta 55, 3355–3367.
Guérin, C., 1980. Les Rhinocéros (Mammalia-Perissodactyla) du Miocène Terminal au Pléistocène supérieur d'Europe Occidentale. Comparaison avec les espèces actuelles. Doc. Lab. Geol. Lyon, Sci. Terre 79, 1–1185.
Guillem-Calatayud, P., 2000. Secuencia climática del Pleistoceno Medio final y del Pleistoceno superior inicial en la fachada central mediterránea a partir de micromamíferos (Rodentia e Insectivora). Saguntum 32, 9–30.
Hanquet, C., 2011. Evolution des paléoenvironnements et des paleoclimats au Pléistocène moyen, en Europe méridional, d'après les faune de micro-mammifères (Ph.D. thesis). Univ. Montpellier III-Paul Valéry.
Harting, P., 1852. De bodem onder Amsterdam onderzocht en beschreven. In: Verhandelingen 1e klas Koninklijke Nederlands Instituut van Wetenschappen, pp. 282–290, 2eReeks 8.
Hearty, P.J., Olson, S.L., Kaufman, D.S., Edwards, R.L., Cheng, H., 2004. Stratigraphy and geochronology of pitfall accumulations in caves and fissures, Bermuda. Quat. Sci. Rev. 23, 1151–1171.
Hodge, E.J., Richards, D.A., Smart, P.L., Andreo, B., Hoffmann, D.L., Mattey, D.P., González-Ramón, A., 2008. Effective precipitation in southern Spain (~266 to 46 ka) based on a speleothem stable carbon isotope record. Quat. Res. 69, 447–457.
Huntley, D.J., Lamothe, M., 2001. Ubiquity of anomalous fading in K-feldspars and the measurement and correction for it in optical dating. Can. J. Earth Sci. 38, 1093–1106.
ICSN, 2011. The International Code for Starch Nomenclature. http://fossilfarm.org/ICSN/Code.html (accessed 30.08.14.).
Ivanovich, M., Harmon, R.S., 1992. Uranium-series Disequilibrium: Application to Earth, Marine and Environmental Sciences, second ed. Clarendon Press, Oxford.
Kahlke, R.D., 1999. The History of the Origin, Evolution and Dispersal of the Late Pleistocene *Mammuthus-Coelodonta* Faunal Complex in Eurasia (Large Mammals). Fenske Companies, Rapid City.
Kahlke, R.D., Kaiser, T.M., 2011. Generalism as a subsistence strategy: advantages and limitations of the highly flexible feeding traits of Pleistocene *Stephanorhinus hundsheimensis* (Rhinocerotidae, Mammalia). Quat. Sci. Rev. 30, 2250–2261.
Kaufman, D.S., 2000. Amino acid racemization in ostracodes. In: Goodfriend, G., Collins, M., Fogel, M., Macko, S., Wehmiller, J. (Eds.), Perspectives in Amino Acid and Protein Geochemistry. Oxford University Press, New York, pp. 145–160.
Kaufman, D.S., Manley, W.F., 1998. A new procedure for determining DL amino acid ratios in fossils using reverse phase liquid chromatography. Quat. Geochronol. 17, 987–1000.
Kolfschoten, T. van, 2000. The Eemian mammal fauna of central Europe. Neth. J. Geo. Sci. 79, 269–281.
Lalueza, C., Pérez-Pérez, A., Turbón, D., 1996. Dietary inferences through buccal microwear analysis of Middle and Upper Pleistocene human fossils. Am. J. Phys. Anthropol. 100, 367–387.
Laplana, C., Blain, H.-A., Sevilla, P., Arsuaga, J.L., Baquedano, E., Pérez-González, A., 2013. Un assemblage de petits vertébrés hautement diversifié à la fin du MIS 5 dans un environnement montagnard au Centre de l'Espagne (Cueva del Camino, Pinilla del Valle, Communauté Autonome de Madrid). Quaternaire 24, 207–216.
López-García, J.M., 2008. Evolución de la diversidad taxonómica de los micromamíferos en la Península Ibérica y cambios paleoambientales durante el Pleistoceno Superior (Ph. D. thesis). Univ. Rovira i Virgili.
López-García, J.M., 2011. Los micromamíferos del Pleistoceno superior de la Península Ibérica. In: Evolución de la diversidad taxonómica y cambios paleoambientales y paleoclimáticos. Académica Español, Saarbrücken.
López-García, J.M., Blain, H.-A., Cuenca-Bescós, G., Arsuaga, J.L., 2008. Chronological, environmental and climatic precisions on the Neanderthal site of the Cova del Gegant (Sitges, Barcelona, Spain). J. Hum. Evol. 55, 1151–1155.
López-García, J.M., Blain, H.-A., De Marfà, R., Garcia, A., Martinell, J., Bennàsar, M.Ll, Cuenca-Bescós, G., 2011. Small mammals from the middle Pleistocene layers of the Sima del Elefante (Sierra de Atapuerca, Burgos, northwestern Spain). Geol. Acta 9, 21–43.
López-García, J.M., Blain, H.-A., Burjachs, F., Ballesteros, A., Allué, E., Cuevas-Ruíz, G.E., Rivals, F., Blasco, R., Morales, J.I., Rodríguez Hidalgo, A., Carbonell, E., Serrat, D., Rosell, J., 2012. A multidisciplinary approach to reconstructing the chronology and environment of southwestern European Neanderthals: the contribution of Teixoneres cave (Moià, Barcelona, Spain). Quat. Sci. Rev. 43, 33–44.
López-García, J.M., Blain, H.-A., Julià, R., Maroto, J., 2014. Environment and climate during MIS 7 and their implications for the late Middle Pleistocene hominins: the contribution of Mollet cave, Serinyà, Girona, northeastern Spain. Quat. Int. 337, 4–10.
Madella, M., Alexandre, A., Ball, T., 2005. International code for phytolith nomenclature 1.0. Ann. Bot-London 96, 253–260.
Manceau, V., Crampe, J.P., Boursot, P., Taberlet, P., 1999. Identification of evolutionary significant units in the Spanish wild goat, *Capra pyrenaica* (Mammalia, Artiodactyla). Anim. Conserv. 2, 33–39.

Markova, A.K., 2000. The Mikulino (= Eemian) mammal faunas of the Russian Plain and Crimea. Geol. Mijnb./Neth. J. Geosci. 79, 293–301.
Maroto, J., Julià, R., López-García, J.M., Blain, H.-A., 2012. Chronological and environmental context of the Middle Pleistocene human tooth of Mollet cave (Serinyà, NE Iberian Peninsula). J. Hum. Evol. 62, 655–663.
Martínez del Valle, R., 1996. Fauna del Pleistoceno superior en el País Valenciano. Aspectos económicos, huellas de manipulación y valoración paleoambiental (Ph. D. thesis). Univ. València.
Martínez del Valle, R., 2001. Els grans mamífers plistocènics. Una aproximació paleoambiental i biostratigràfica. In: Villaverde, V. (Ed.), De Neandertals a Cromanyons. L'inici del poblament humà a les terres valencianes. Univ. València, pp. 45–56.
Mazza, P., 1988. The Tuscan Early Pleistocene rhinoceros. *Dicerorhinus etruscus*. Paleontogr. Ital. 75, 1–87.
Mazza, P., Sala, B., Fortelius, M., 1993. A small latest Villafranchian (late Early Pleistocene) rhinoceros from Pietrafitta (Perugia, Umbría, Central Italy) with notes on the Pirro and Westerhoven rhinoceroses. Palaeontogr. Ital. 80, 25–50.
Middleton, W.D., Rovner, I., 1994. Extraction of Opal phytoliths from herbivore dental calculus. J. Archaeol. Sci. 21, 469–473.
Mitchell, B., Staines, B.W., Welch, D., 1977. Ecology of Red Deer: a Research Review Relevant to Their Management in Scotland. Institute of Terrestrial Ecology, NERC, Banchory.
Mlíkovský, J., 2002. Cenozoic Birds of the World. Part 1: Europe. Ninox Press, Prague.
Mol, D., de Vos, J., van der Plicht, J., 2007. The presence and extinction of *Elephas antiquus* Falconer and Cautley, 1847. Quat. Int. 169/170, 149–153.
Morales, J.V., Sanchís, A., 2009. The Quaternary fossil record of the genus *Testudo* in the Iberian Peninsula. Archaeological implications and diachronic distribution in the western Mediterranean. J. Archaeol. Sci. 36, 1152–1162.
Moriarty, K.C., McCulloch, M.T., Wells, R.T., McDowell, M.C., 2000. Mid-Pleistocene cave fills, megafauna remains and climate change at Naracoorte, South Australia: towards a predictive model using U-Th dating speleothems. Palaeogeogr. Palaeoclimatol. Palaeoecol. 159, 113–143.
Mourer-Chauviré, C., 1975. Les oiseaux du Pléistocène moyen et supérieur de France. Doc. Lab. Fac. Sci. Lyon 64, 624.
Muñoz-García, M.B., Martín-Chivelet, J., Rossi, C., Ford, D.C., Schwarcz, H.P., 2007. Chronology of Termination II and the Last Interglacial Period in North Spain based on stable isotope records of stalagmites from Cueva del Cobre (Palencia). J. Iber. Geol. 33, 17–30.
Nabais, M., 2010. Middle Palaeolithic Tortoise use at Gruta da Oliveira (Torres Novas, Portugal) (MSc dissertation). Univ. College London.
Nambi, K.S.V., Aitken, M.J., 1986. Annual dose conversion factors for TL and ESR dating. Archaeometry 28, 202–205.
Nesbitt, H.W., Young, G.M., McLennan, S.M., Keays, R.R., 1996. Effects of chemical weathering and sorting on the petrogenesis of siliciclastic sediments, with implications for provenance studies. J. Geol. 104, 525–542.
Orlando, L., Mashkour, M.A., Burke, Douady, C.J., Eisenmann, V., Hänni, C., 2006. Geographic distribution of an extinct equid *Equus hydruntinus*: Mammalia, Equidae) revealed by morphological and genetical analyses of fossils. Molec. Ecol. 15, 2083–2093.
Ortiz, J.E., Torres, T., Delgado, A., Julià, R., Llamas, F.J., Soler, V., Delgado, J., 2004. Numerical dating algorithms of amino acid racemization ratios analyzed in continental ostracodes of the Iberian Peninsula (Spain). Application to Guadix-Baza Basin (southern Spain). Quat. Sci. Rev. 23, 717–730.
Ortiz, J.E., Torres, T., Delgado, A., Reyes, E., Díaz-Bautista, A., 2009. A review of the Tagus river tufa deposits (central Spain): age and palaeoenvironmental record. Quat. Sci. Rev. 28, 947–963.
Pike, A.W.G., Hedges, R.E.M., Van Calsteren, P., 2002. U-series dating of bone using the diffusion-adsorption model. Geochim. Cosmochim. Acta 66, 4273–4286.
Pike, A.W.G., Eggins, S., Grün, R., Hedges, R.E.M., Jacobi, R.M., 2005. U-series dating of the Late Pleistocene fauna from Wood Quarry (Steetley), Notinghamshire, UK. J. Quat. Sci. 20, 59–65.
Piperno, D.R., 2006. Phytoliths: a Comprehensive Guide for Archaeologists and Paleoecologists. AltaMira Press, Lanham.
Plagnes, V., Causse, C., Genty, D., Paterne, M., Blamart, D., 2002. A discontinuous climatic record from 187 to 74 ka from a speleothem of the Clamouse Cave (south of France). Earth Planet. Sci. Lett. 201, 87–103.
Rink, W.J., 1997. Electron spin resonance (ESR) dating and ESR applications in quaternary science and archaeometry. Rad. Meas. 27, 975–1025.
Rivas-Martínez, S., 1987. Memoria del mapa de series de vegetación de España. Ministerio de Agricultura, Pesca y Alimentación, Madrid.
Rivas-Martínez, S., Rivas-Sáenz, S., 1996-2009. Worldwide Bioclimatic Classification System. www.globalbioclimatics.org.
Rosenbauer, R.J., 1991. UDATE1: a computer program for the calculation of uranium -series isotopic ages. Comput. Geosci. 17, 45–75.
Rouzaud, F., Soulier, M., Brugal, J.P., Jaubert, J., 1990. L'Igue des Rameaux (Saint-Antonin-Noble-Val, Tarn-et-Garonne). Un nouveau gisement du pléistocène moyen. Premiers résultats. Paléo 2, 89–106.
Rosell, J., Blasco, R., Rivals, F., Chacón, M.G., Menéndez, L., Morales, J.I., Rodríguez-Hidalgo, A., Cebrià, A., Carbonell, E., Serrat, D., 2010. A stop along the way: the role of Neanderthal groups at layer III of Teixoneres Cave (Moià, Barcelona,Spain). Quaternaire 21, 139–154.
Sala, B., Fortelius, M., 1993. The rhinoceros of Isernia La Pineta (early Middle Pleistocene, Southern Italy). Palaeontogr. Ital. 80, 157–174.
Sánchez Goñi, M.F., Eynaud, F., Turon, J.L., Shackleton, N.J., 1999. High resolution palynological record off the Iberian margin: direct land–sea correlation for the LastInterglacial complex. Earth Planet Sc. Lett. 171, 123–137.
Sánchez Goñi, M.F., Bakker, P., Desprat, S., Carlson, A.E., van Meerbeeck, C.J., Peyron, O., Naughton, F., Fletcher, W.J., Eynaud, F., Rossignol, L., Renssen, H., 2012. European climate optimum and enhanced Greenland melt during the Last Interglacial. Geology 40, 627–630.
Sánchez Goñi, M.F., Bard, E., Landais, A., Rossignol, L., d'Errico, F., 2013. Air–sea temperature decoupling in western Europe during the last interglacial–glacial transition. Nat. Geo. Sci. 6, 837–841.
Sánchez Marco, A., 1987. Saalian s.l. avian findings in the northern Iberian Plateau. In: Mourer-Chauviré, C. (Ed.), L'évolution des oiseaux d'après le témoignage des fossiles, Doc. Lab. Geol. Lyon 99, pp. 193–196.
Sánchez Marco, A., 1995. Las aves de la unidad estratigráfica TG-11 de la Galería (sierra de Atapuerca, Burgos, España). In: Actas de Evolución humana en Europa y los yacimientos de la Sierra de Atapuerca. Junta de Castilla y León, Valladolid, pp. 137–146.
Sánchez Marco, A., 1999a. Aves del yacimiento mesopleistoceno de Galería (sierra de Atapuerca). Patrones ecológicos en el Pleistoceno medio. In: Carbonell, E., Rosas, A., Díez, J.C. (Eds.), Atapuerca: ocupaciones humanas y paleoecología del yacimiento de Galería, Arqueología en Castilla y León 7, pp. 211–224.
Sánchez Marco, A., 1999b. Implications of the avian fauna for paleoecology in the Early Pleistocene of the Iberian peninsula. J. Hum. Evol. 37, 375–388.
Sánchez Marco, A., 2004. Avian zoogeographical patterns during the Quaternary in the Mediterranean region and paleoclimatic interpretation. Ardeola 51, 91–132.
Sánchez Marco, A., 2005. Aves del Plioceno superior de la meseta sur ibérica: una asociación ornítica aparentemente cuaternaria. Rev. Esp. Paleontol. 20, 143–157.
Sánchez Marco, A., 2007. New occurrences of the extinct vulture *Gyps melitensis* (Falconiformes, Aves) and a reappraisal of the paleospecies. J. Vert. Paleont. 27 (4), 1057–1061.
Sanz, M., 2013. Patrons d'acumulació de restes de fauna del Plistocè superior al nord-est peninsular (àrea del Massís del Garraf-Ordal) (Ph.D. thesis). Univ. Barcelona.
Sanz, M., Daura, J., Brugal, J.-P., 2014. First occurrence of the extinct deer *Haploidoceros* in the Iberian Peninsula in the Upper Pleistocene of the Cova del Rinoceront (Castelldefels, Barcelona). CR. Palevol. 13, 27–40.
Sanz, M., Daura, J., Terrado, E., Méndez, M., Fullola, J., 2011. La GeotecniaVertical aplicada a la rehabilitación de yacimientos Pleistocenos. Treb. Mus. Geol. Barc. 18, 25–35.
Schulte, L., Julià, R., Burjachs, F., Hilgers, A., 2008. Middle Pleistocene to Holocene geochronology of the River Aguas terrace sequence (Iberian Peninsula): fluvial response to Mediterranean environmental change. Geomorphology 98, 13–33.
Sesé, C., Panera, J., Rubio-Jara, S., Pérez-González, A., 2011. Micromamíferos del Pleistoceno Medio y Pleistoceno Superior en el Valle del Jarama: yacimientos de Valdocarros y HAT (Madrid, España). Estud. Geol. 67, 131–151.
Shackleton, N.J., Sanchez-Goni, M.F., Pailler, D., Lancelot, Y., 2003. Marine Isotope Substage 5e and the Eemian Interglacial. Glob. Planet. Change 36, 151–155.
Staller, J.E., Thompson, R.G., 2002. A multidisciplinary approach to understanding the initial introduction of maize into Coastal Ecuador. J. Archaeol. Sci. 29, 33–50.
Strömberg, C.A.E., Werdelin, L., Friis, E.M., Saraç, G., 2007. The spread of grass-dominated habitats in Turkey and surrounding areas during the Cenozoic: phytolith evidence. Palaeogeogr. Palaeoclimatol. Palaeoecol. 250, 18–49.
Stuart, A.J., 2005. The extinction of woolly mammoth (*Mammuthus primigenius*) and straight-tusked elephant (*Palaeoloxodon antiquus*) in Europe. Quat. Int. 126–128, 171–177.
Stuart, A.J., Sulerzhitsky, L.D., Orlova, L.A., Kuzmin, Y.V., Lister, A.M., 2002. The latest woolly mammoths (*Mammuthus primigenius* Blumenbach) in Europe and Asia: a review of the current evidence. Quat. Sci. Rev. 21, 1559–1569.
Tissoux, H., Falguères, Ch, Bahain, J.-J., Rosell, J., Cebrià, A., Carbonell, E., Serrat, D., 2006. Datation per les séries de l'Uranium des occupations moustériennes de la grotte des Teixoneres (Moià, province de Barcelone, Espagne). Quaternaire 17, 27–33.
Torres, T., Llamas, J., Canoira, L., García-Alonso, P., García-Cortés, A., Mansilla, H., 1997. Amino acid chronology of the Lower Pleistocene deposits of Venta Micena (Orce, Granada, Andalusia, Spain). Org. Geoch 26, 85–97.
Trinkaus, E., Marks, A.E., Brugal, J.P., Bailey, S.E., Rink, W.J., Richter, D., 2003. Later middle Pleistocene human remains from the Almonda karstic system, Torres Novas, Portugal. J.Hum. Evol. 45, 219–226.
Tyrberg, T., 1998. Pleistocene Birds of the Palearctic: a Catalogue. In: Publ. Nuttall Ornithological Club 27. Massachusetts, Cambridge.
Ureña, I., Arsuaga, J.L., Galindo-Pellicena, M.A., Götherström, A., Valdiosera, C., 2011. Filogenia y evolución local de la cabra montés (*Capra pyrenaica*) en el yacimiento Cuaternario de Chaves (Huesca, España). Bol. R. Soc. Esp. Hist. Nat. Sec. Geol. 105, 5–14.
van der Made, J., 2010. The rhinos from the Middle Pleistocene of Neumark-Nord (Saxony-Anhalt). In: Mania, D., Meller, H. (Eds.), Ein interglaziales Ökosystem des mittelpaläolithischen Menschen: Halle (Saale), Landesmuseum für Vorgeschichte, Veröffentlichungen des Landesamtes für Denkmalpflege und Archäologie Sachsen-Anhalt. 62, pp. 433–527.
Vicente, J., 1965. Brecha osífera cuaternaria en el macizo de Garraf (Barcelona). Bol. Sec. Est. Cent. Exc. Puig Castellar 1, 9–10.
Vidal-Matutano, P., Hernández, C.M., Galván, B., Mallol, C., 2015. Neanderthal fire-wood management: evidence from Stratigraphic Unit IV of Abric del Pastor (Eastern Iberia). Quat. Sci. Rev. 111, 81–93.

Villalta, J.F de, Crusafont, M., 1950. Un nuevo yacimiento pleistocénico en Castelldefels. Nota preliminar. Estud. Geol. 6, 275–285.
Wainer, K., Genty, D., Blamart, D., Daëron, M., Bar-Matthews, M., Vonhof, H., Dublyansky, Y., Pons-Branchu, E., Thomas, L., van Calsteren, P., Quinif, Y., Caillon, N., 2011. Speleothem record of the last 180 ka in Villars cave (SW France): Investigation of a large δ18O shift between MIS6 and MIS5. Quat. Sci. Rev. 30, 130–146.
Wehmiller, J.F., 1984. Interlaboratory comparison of amino acid enantiomeric ratios in fossil mollusks. Quat. Res. 22, 109–120.
Wehmiller, J.F., Miller, G., De Vogel, S., Kaufman, D.S., Bright, J., Murray-Wallace, C.V., Ortiz, J.E., Penkman, K., 2010. Interlaboratory comparison of amino acid D/L values. In: Geological Society of America Annual Meeting, Denver, Abstracts with Programs 42, p. 86.
Yang, X., Perry, L., 2013. Identification of ancient starch grains from the tribe Triticeae in the North China Plain. J. Archaeol. Sci. 40, 3170–3177.
Yang, X., Zhang, J., Perry, L., Wan, Z., Li, M., Diao, X., Lu, H., 2012. From the modern to the archaeological: starch grains from millets and their wild relatives in China. J. Archaeol. Sci. 39, 247–254.
Zimmerman, D.W., 1971. Thermoluminescence dating using fine grain from pottery. Archaeometry 13, 29–52.